university of groningen / faculty of mathematics and natural sciences

Applied physics master thesis

Hydrogenation of polycyclic aromatic hydrocarbons

By
Nolan Foley
s1929046

August 2016

Supervisors:
prof. dr. ir. R.A. Hoekstra
dr. T.A. Schlathölter

Table of contents

Introduction

Molecular hydrogen is the most abundant molecule in the universe and plays a key role in many astrophysical processes. As such, understanding the processes that lead to its formation is of great interest. A number of potential formation processes have already been explored. While gas phase routes to H_2 formation have been found to be inefficient, formation on interstellar dust grains has been identified as one possible mechanism [1,2]. Another possible route to molecular hydrogen formation is on interstellar polycyclic aromatic hydrocarbons (PAHs) [3,4,5,6,7]. Atomic hydrogen can adsorb onto these PAHs, leaving them in a state of superhydrogenation. It has been proposed that hydrogenated PAHs are indeed present in space [8,9].

If a hydrogen atom impinges on a position of the PAH that has already got an additional H attached, an Eley-Rideal reaction can occur [6,10]. Here the impinging atom and one of the hydrogen atoms attached to the molecule bind and abstract from the PAH as molecular hydrogen.

The viability of this route, however, remains unclear [6,10]. It has been calculated that for neutral coronene, deposited on a surface, the reaction cross-section for such an abstraction reaction was around 1/20th of the cross-section for addition reactions of hydrogen on the molecule [6], implying a relatively low occurrence of these abstraction reactions. However, there are differences between the hydrogenation of neutral coronene and coronene cations [11], and it is possible that coronene in gas phase, a closer approximation to the conditions in the interstellar medium, will behave differently to coronene in a thin film.

Aside from these abstraction processes, the attachment process of hydrogen on PAH itself still has not been entirely explored. It is for instance possible that atomic hydrogen that has been attached during the hydrogenation process can desorb from the PAH, influencing the observed rate of hydrogenation. Further, each hydrogen atom impinging on the PAH deposits energy into the molecule, possibly leading to fragmentation unless the molecule disperses the energy through for instance infrared emission or electron emission. The effects of the rate of hydrogenation are therefore also of interest.

The purpose of this thesis is to investigate these various aspects of the attachment and abstraction processes of hydrogen on PAHs in gas phase. Specifically, the following questions are addressed:

- Does atomic hydrogen desorb from a hydrogenated PAH?
  Understanding whether desorption occurs and the mechanics behind it would give an insight into the rate of hydrogenation that has occurred on a given molecule and the measured hydrogenation after a given period of time. This is especially relevant for achieving higher states of hydrogenation, as those either require higher rate of incoming hydrogen atoms, or longer hydrogenation periods, which could potentially lead to a degree of loss of hydrogenation due to desorption.

- How does the hydrogenation rate affect the fragmentation of PAHs?
  Each impinging hydrogen atom deposits a certain energy into the molecule. A PAH can usually lose this energy through IR emission. A higher rate of impingement leads to more energy being deposited in a shorter amount of time, which could lead to the molecule fragmenting, due to it not being able to lose the energy at the same rate. This can be seen as the flip side to the desorption when it comes to achieving high hydrogenation states; long

hydrogenation times could lead to higher occurrence of desorption, leading to a possible loss of the highest hydrogenation states, while shorter hydrogenation times at higher impingement rates could lead to higher fragmentation of coronene molecules, and thus overall loss of signal.

- At what rate does molecular hydrogen abstract from hydrogenated PAHs?
  During hydrogenation experiments it can be challenging to estimate the occurrence of abstraction, as the resulting mass difference can not be told apart from a PAH which only reached a lower state of hydrogenation. Nonetheless, a proper understanding of this process and its occurrence is essential for a complete overview of the hydrogenation process, and potentially piecing together the puzzle of natural hydrogen gas formation in the interstellar medium. In order to measure the occurrence of this process, the coronene was exposed to deuterium atoms, rather than hydrogen atoms, as the mass difference between deuterium and the hydrogen already present on the molecule would be measurable.

Coronene was used as the sample PAH. It should be noted that coronene is not a major species in the interstellar medium [4], but it has frequently been used as sample PAH in related research [7,10,11,12,13,14,15] due to it being fairly large and having a compact shape, making it relatively easy to work with. It is also the largest PAH that is commercially readily available. It consists of 24 C atoms and 12 H atoms, forming 7 hexagonal rings, where the outermost 12 C atoms each have 1 H atom attached. The chemical structure can be seen in figure 1.

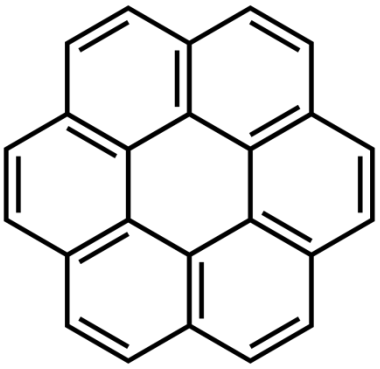

Figure 1: The chemical structure of coronene (source: ref. 16)

Experimental setup

A crucial step in studying a PAH in conditions resembling those of the interstellar medium is bringing it into the gas phase. Studying PAHs in a solid or as a film reduces the freedom of deformation of the molecule, restricts access to the underside of these flat molecules and the surface acts as a heat bath, potentially compromising the results. However, under standard conditions, PAHs are a solid substance, so in order to study them in the gas phase they must be dissolved and ionised, and subsequently electrosprayed into a vacuum system where electric fields guide the ions to enable studying them. All experiments are carried out at ambient temperature.

The samples are studied in a home-built experimental setup known as “Paultje”, named after the Paul type ion trap at its centre. A diagram of the internal components of Paultje can be seen in figure 2. The sample is put into a clean syringe, which is mounted in an electronic syringe pump, regulating the flow of the solution to 0.10 ml/hour. The solution is electrosprayed from a needle, through a capillary tube and into a radio frequency ion funnel. Here a series of 26 plates, alternatingly positively or negatively charged and with a decreasing diameter of hole in their centres, guides the stream of ions into a tight beam, which enters an RF octopole. From here the beam of ions goes through RF quadrupole mass filter, which was set to only allow particles with a mass/charge ratio of 300:1 through, so specifically singly-charged coronene. However, there is always a compromise between retaining signal strength and filtering out as many other masses as possible, so in practise it is unavoidable that some unwanted masses get through. In the case of coronene, the isotope peak at 301 mass is the by far the largest unwanted mass peak. Coronene consists of 24 C and 12 H atoms, and given the natural abundance of the C-13 and deuterium isotopes to C-12 and H respectively, there is a roughly 25% chance that a given coronene molecule will have mass 301, and it is very difficult to filter out such a small difference with the mass filter.

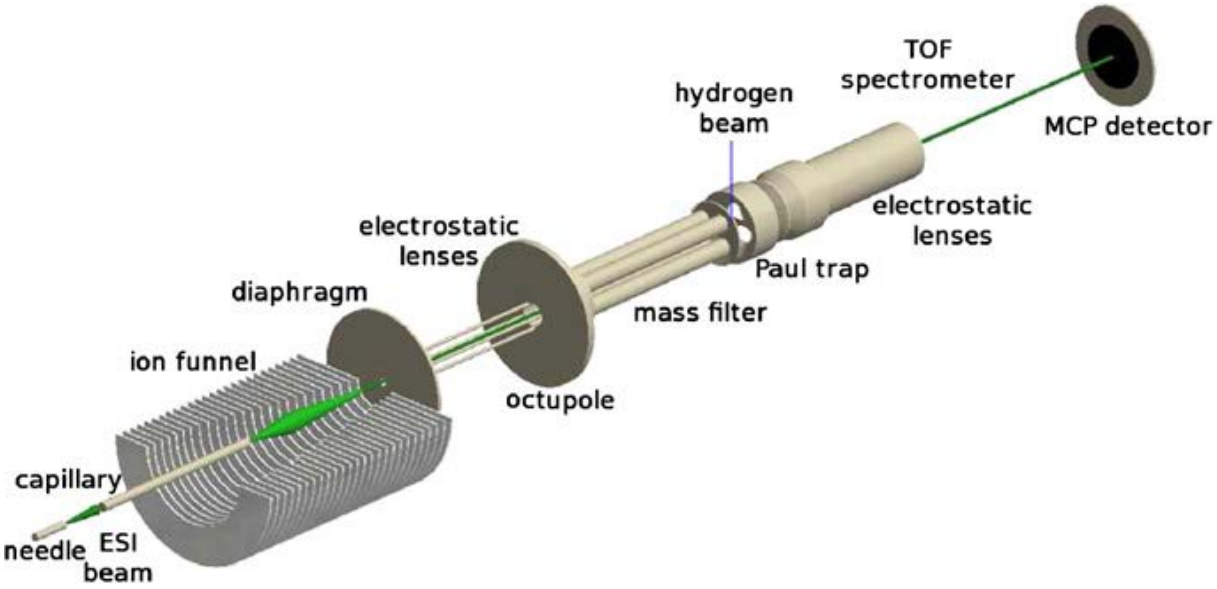

Figure 2: Diagram of "Paultje" (source: adapted from ref. 7)

From the mass filter the remaining ions are guided into the 3D ion trap, where they are held in an RF field. This is where the hydrogenation or deuteration of the sample can take place. Finally, the sample is extracted from the ion trap by applying a high voltage to the cap electrodes of the trap,

positive on the side of the mass filter, and negative on the other side. This ejects the PAH cations from the trap, through a set of electrostatic lenses, accelerating it towards a detector consisting of a set of micro-channel plates (MCPs) at the far end of a time-of-flight (TOF) tube. The ions arrive at the detector, and their time of flight is measured, which is converted into a mass/charge ratio. The singly charged coronene cations in the sample are not subject to any charge changing processes, so in this case the spectrum of mass/charge ratios simply becomes a mass spectrum. This spectrum is analysed to determine what the ratios are between different hydrogenation states of the coronene, and in the case there is fragmentation it is likewise used to determine in what manner and what fraction of the coronene has fragmented.

The studied samples were prepared in the following manner:

1. A saturated solution of coronene in methanol is made, which can function as a stock solution for a series of measurements.
2. This stock solution is centrifuged at 14000 rpm for 5 minutes, to ensure all precipitate has sunk to the bottom.
3. From the top of the stock solution 650 µl of solution is pipetted, and deposited into a new 1 ml sample cup.
4. The stock solution is refilled to its original volume by simply adding 650 µl of methanol. The saturation of the stock solution can easily be verified by the presence of a bright yellow precipitate after shaking. This ensures the reusability of the stock solution for creating future samples.
5. 50 µl of 5 mM $Zn(NO_3)_2$ in methanol solution is added to the sample cup, which acts as an ionisation agent to the coronene, taking up 1 electron to form coronene cations.
6. 300 µl of methanol is added to the sample cup to bring the sample volume up to 1 ml. The sample is now ready for use.

The hydrogen source used to create the atomic hydrogen and deuterium is a Slevin-type source. H_2 gas is pumped from a 12 bar minican, through a glass tube, and finally into the ion trap by means of a Teflon guiding tube. The glass tube is water-cooled through a second layer of glass, and is surrounded by a large copper coil, which is connected to a 27 MHz RF source. When this RF source is switched on, the radio frequency electric field produced by the coil dissociates the H_2 gas into atomic hydrogen. This results in a discharge, producing a visible purple glow. The water cooling on the glass tube reduces the discharge temperature and inhibits recombination [17]. When switched off, the H_2 gas simply flows through the tube. The H_2 gas is non-reactive under these circumstances, and while it may impinge upon sample molecules being held in the ion trap, it will simply be extracted from the vacuum chamber by the pumps. The dissociated hydrogen gas, however, is used to hydrogenate samples. The hydrogenation time of samples can therefore be accurately controlled by switching the RF source on and off.

The rate of hydrogenation is controlled by the flow of the hydrogen gas through the glass tube. By comparing the pressures in the ion trap chamber with and without the hydrogen gas flowing it is possible to deduce a parameter indicative of the rate of the flow, and with that the rate of hydrogenation of the sample. Typical pressures in the chamber are 10^{-7} mbar without hydrogen flowing, and between 10^{-6} to 10^{-5} mbar with hydrogen flowing.

The hydrogen source was originally used in crossed-beam experiments in the 1980s. It was revived in 2012 by Leon Boschman [7] after a period of disuse, in order to hydrogenate gas phase coronene. While it was successful in doing so, it was modified and rebuilt quickly so it would simply work. This resulted in many tubes supporting their own weight, while the hydrogen gas bottle was connected by plastic tubing, which is prone to leaking. Furthermore, the setup is regularly disassembled, transported, and reassembled. As more hydrogenation experiments were set to begin, it was necessary to rebuild the source in a more reliable and structurally sound manner.

In order to do this, a more permanent method of attachment for the tubing and valves to the source was designed. A metal structure was designed that could be bolted securely on to the side of the base of the source, and all the valves, tubing and other attachments could be attached to this structure by means of carefully placed bolt holes. The design schematic of this frame can be seen in figure 3.

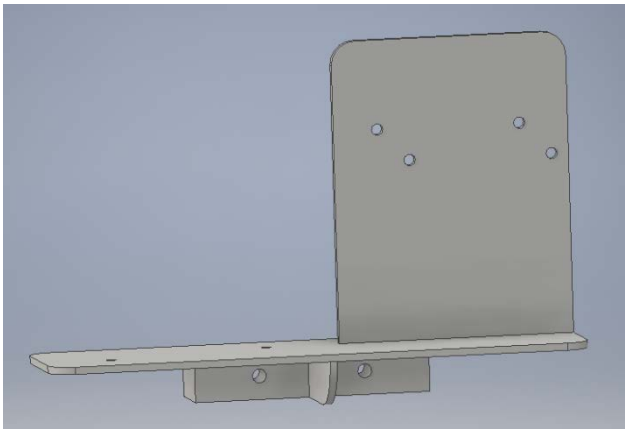

Figure 3: Design schematic of the metal structure that was to act as a base for the hydrogen source attachments

The whole system was to be more compact, rigid, airtight, and more accurate through the inclusion of a mass flow controller (MFC). Naturally, however, complications arose during the process of construction and taking into operation.

The biggest issue was encountered while testing the setup after assembly. The mass flow controller, a key component in the H-source, was designed for higher gas flows than the vacuum pumps on Paultje can handle while retaining the operating pressures in the trap chamber and TOF tube. Original estimates suggested that the lower end of the MFC's flow range would suffice for reaching the pressures required for the operation of Paultje, but in practise this was not the case. A pressure of around 10^{-5} mbar could be reached in the trap chamber, which is on the upper limit of operating pressures. Operating at this flow of hydrogen gas would, however, limit experiments to high atomic hydrogen flow measurements, which are not always desirable, and could put the sensitive MCPs at risk, which is always undesirable.

This issue was solved by installing a needle valve system in place of the MFC. The needle valve has the advantage of being able to reach both high and very low gas flow levels, and as such allows for many kinds of experiments. Nonetheless, an MFC designed for very low gas flows would be a preferable solution, as they are digitally programmable, highly consistent in their throughput and have a nicely sealing valve, while needle valves are fragile, somewhat tricky to manually set, and this particular one could not fully close, necessitating a sealing valve elsewhere in the system.

The hydrogen source is partly sealed with a number of o-rings, and in order to ensure their proper functioning some vacuum grease is required. In most cases the relatively cheap L-type Apiezon would suffice, but one ring is in contact with a small tank for liquid nitrogen, used for cooling the atomic hydrogen flow to reduce recombination. As such, the author deemed it wise to order vacuum grease capable of withstanding cryogenic temperatures. It then emerged that the tank was a vestigial component from when the hydrogen source was originally constructed and would not be used, and that regular vacuum grease would therefore suffice. The N-type Apiezon lies unopened, awaiting future experiments at low temperatures.

A fair length of Swagelok tubing was used and recycled from old, disassembled systems. While this aspect of construction was challenging, the resulting tubing was highly compact and solid. Upon connecting the rebuilt source to Paultje and attempting to pump down to vacuum, it emerged that the tubing was also far from airtight. It took a lot of tightening and a few last-minute adjustments to ensure the entire system was properly sealed, which was made significantly more complicated by the highly compact and solidly mounted design.

Aside from these issues, however, the upgrade was a fairly clean process. The result is almost as first envisioned, aside from the MFC having been replaced by a needle valve. A picture of the setup, which still included the MFC at the time, can be seen in figure 4. The tubing and valves are securely mounted on a solid frame, which can be attached and detached from the main body of the source. Pressures of 10^{-7} mbar have been reached in the trap chamber. The hydrogen gas bottle can be attached to a pressure regulator, which feeds through to the pin valve. From there, the gas can either go directly into the trap chamber through a dedicated outgassing valve, or be fed into the RF source, where it can be split into atomic hydrogen and subsequently guided onto the sample in the trap. The gas in the RF source is cooled by a water cooling system, which can be attached to Paultje separately, but requires an external 12V source to power the pump. The RF source is powered by an external amplifier, and can be switched on or off by a signal from the controlling computer. The hydrogen gas flow is constant, but the dissociation into atomic hydrogen is regulated by the RF source.

Figure 4: The hydrogen source mounted on Paultje. This photo was taken with the MFC still in place

Experiment 1 – atomic hydrogen desorption

These measurements should give insight into whether attached hydrogen desorbs from hydrogenated coronene under the neutral conditions of being held in the Paul trap. A desorption reaction means that an attached hydrogen atom desorbs from the molecule, and should result in an increase in intensity of lower mass peaks when compared to a spectrum where less desorption is occurring.

For the experiments in this section, a fixed background pressure of hydrogen gas in the Paul trap chamber was set (5.0 * 10^{-6} mbar), and a fixed atomic hydrogen exposure time was used (τ_{exp}= 5 s). This way experimental conditions are comparable and reproducible throughout the experiments.

Four measurements were conducted following the scheme below:

i. A reference mass spectrum of coronene cations, unexposed to atomic hydrogen was recorded.
ii. The coronene sample was exposed to H atoms for τ_{exp}=5 s. The resulting mass spectrum was recorded immediately after exposure (τ_{hold}=0 s).
iii. The coronene sample was exposed to H atoms for τ_{exp}=5 s, and subsequently held in the ion trap for τ_{hold}=10 s before recording the mass spectrum.
iv. The coronene sample was held in the ion trap for τ_{hold}=10 s, and subsequently exposed to H atoms for τ_{exp}=5 s before recording the mass spectrum.

A comparison of mass spectra ii and iii should give information on the occurrence of desorption, as τ_{hold} of the hydrogenated sample increases from 0 s to 10 s. In iv, τ_{hold}=10 s is set *before* the hydrogenation period, to ensure that it is not the time the sample spends in the trap itself that makes a difference, but that any measured effect originates from the hydrogenated sample having time to cool down and undergo some reactions before measurement. For this to be the case, the results from measurements ii and iv must be identical.

The reference measurement can be found in figure 5. Both the 300 amu bare coronene peak and the 301 amu isotope peak can be seen, along with contamination peaks at around 298 and 299 amu, which are present in all subsequent measurements and can be ignored.

The hydrogenation peaks in the mass spectra in this thesis are labelled as “corX” where X is replaced by the number of additional hydrogen atoms attached to the molecule. So, for instance, “corH” indicates the peak for coronene with 1 additional hydrogen attached, and “corH5” indicates the peak for coronene with 5 hydrogen atoms attached.

In figure 6 the observed mass peaks from measurements ii and iv are compared. The peaks are highly similar, but not identical, as a slight decrease in 5-fold hydrogenated coronene can be seen in measurement iv. It is currently unclear as to why this dip in intensity is seen for this mass peak, or what its significance is.

The mass peaks from measurements ii and iii are compared in figure 7. Interestingly the even numbered superhydrogenation mass peaks all remain at identical intensity, while the odd numbered peaks all decrease slightly. Furthermore, the lower mass peaks relatively decrease more, with the

301 mass peak having undergone a significant dip in intensity, while the 303 and 305 mass peak lose less and less intensity.

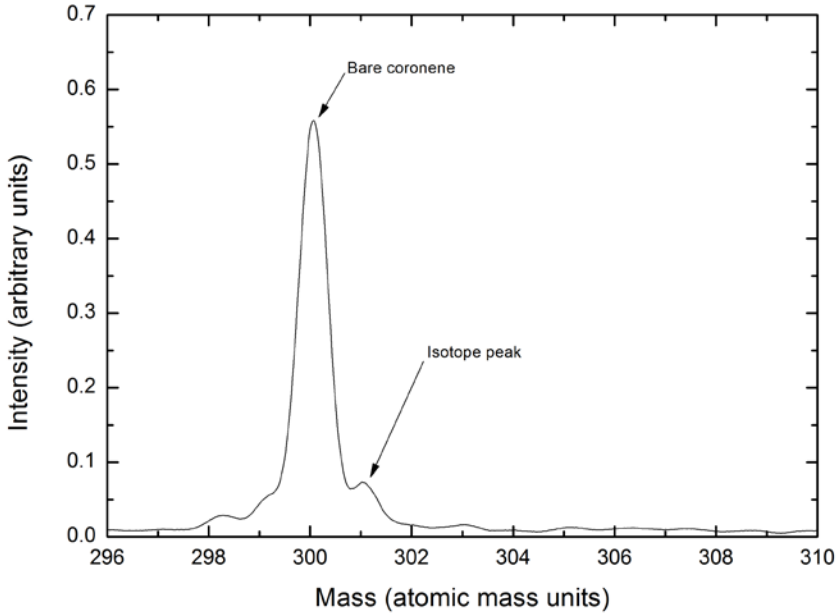

Figure 5: Mass spectrum of measurement i. We see the strong peak at 300 mass for bare coronene, a small peak at 301 for the isotope peak of coronene and two contamination peaks close to 298 and 299 mass units which also appear in all following measurements.

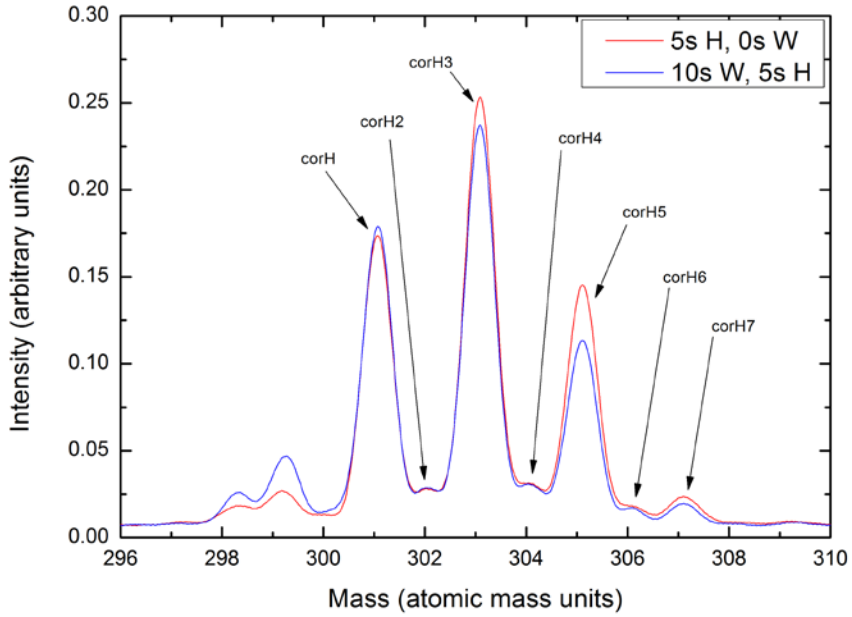

Figure 6: Comparison between measurement ii (coronene exposed to τ_{exp}=5 s of atomic hydrogen) in red, and measurement iv (coronene held in the ion trap for τ_{hold}=10 s before exposure to τ_{exp}=5 s of atomic hydrogen) in blue.

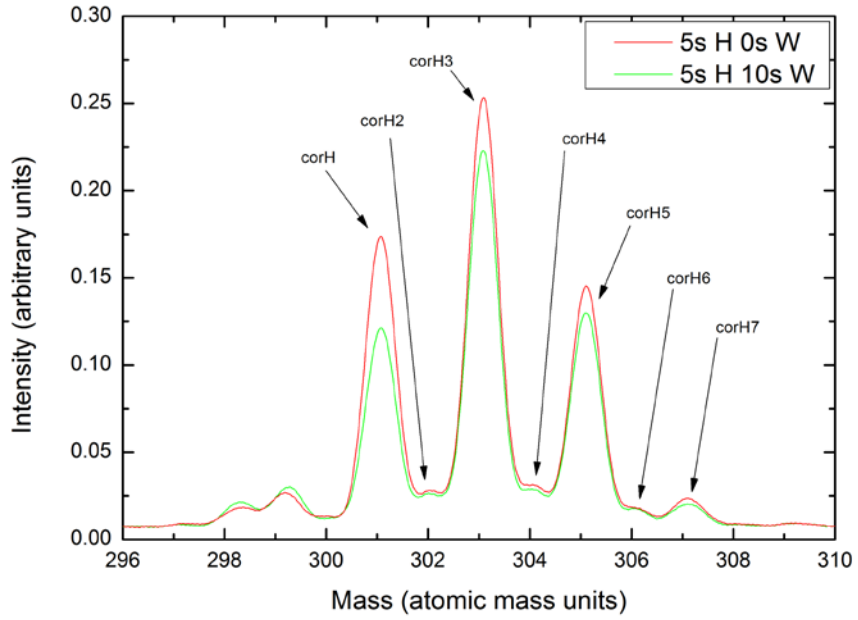

Figure 7: Comparison between measurement ii (coronene exposed to τ_{exp}=5 s of atomic hydrogen) in red, and measurement iii (coronene exposed to τ_{exp}=5 s of atomic hydrogen followed by τ_{hold}=10 s before measurement) in green.

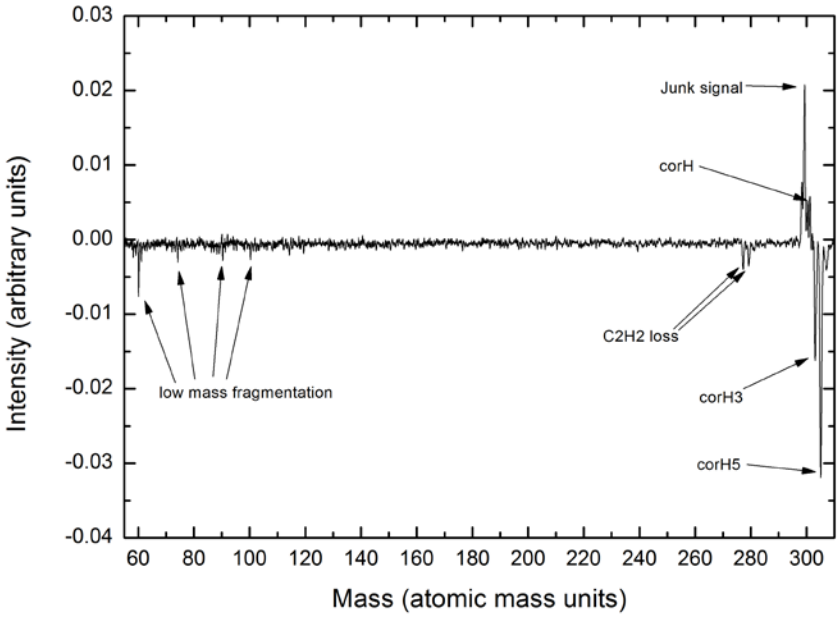

Figure 8: Difference between measurements iv and ii. A positive value indicates measurement iv had a higher peak, a negative value indicates measurement ii had a higher peak.

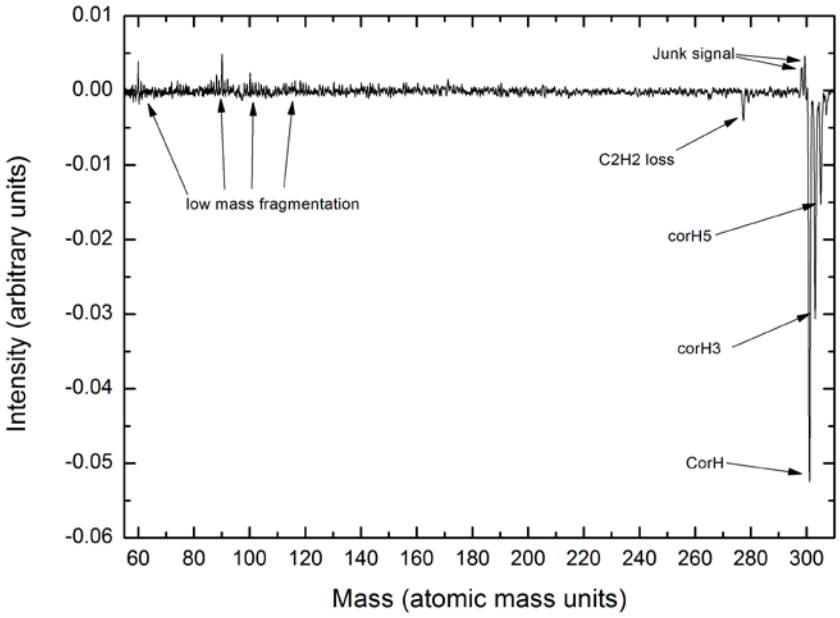

Figure 9: Difference between measurements iii and ii. A positive value indicates measurement iii had a higher peak, a negative value indicates measurement ii had a higher peak.

If the significant dip in intensity for the 301 mass peak was due to a H desorption reaction, the consequence would be a significant increase for the 300 mass peak. As is evidenced by figure 7, however, this is not the case, nor do any of the other even numbered mass peaks appear to undergo any kind of increase. We can conclude from this that desorption is not the main mechanism at play here.

As such, the differences must be sought in the lower mass fragmentation regime. These differences are displayed in figures 8 and 9. Figure 8 shows the difference in peak intensity between measurements ii and iv. From these peaks we can see that measurement iv produced lower peaks overall, except the contamination peaks and the 301 amu peak. In other words, holding the sample in the ion trap appears to result in an overall loss of signal, possibly due to occurrence of charge exchange or loss of ions from the trap over time.

Fig. 9 displays the difference between measurements ii and iii, i.e. the net effect of τ_{hold}=10 s post-hydrogenation. Here we see a loss of signal in measurement iii for the 301, 303 and 305 peaks, and for the C_2H_2 loss peaks, but an increase in peak height for the low mass fragmentation peaks.

The C_2H_2 loss peaks arise from two of the outer edge carbon atoms from one of the benzene rings breaking off. This leads to a loss of mass of 26 units, leaving the remaining molecule at a mass of 274 units plus any mass gained from hydrogenation.

This increase in low mass fragmentation appears to be the result of both the decreased superhydrogenation mass peaks and C_2H_2 loss peaks. It appears, therefore, that the hydrogenated coronene undergoes a higher degree of fragmentation when held in the trap after hydrogenation, beyond C_2H_2 loss. The details of the extra fragmentation require further investigation, as the process behind its formation is as yet unknown.

Experiments – hydrogen fluence variation

The question we set out to answer with these experiments is how the hydrogenation rate affects the fragmentation of PAHs. This is done by varying the rate of flow of the hydrogen gas that hits the sample. For these experiments three flow rates of the gas were used, which were measured by the resulting background pressures in the ion trap chamber. Under operating conditions the typical background pressure in the ion trap chamber without a flow of hydrogen gas is around $1*10^{-7}$ mbar. The three background pressures used as indicator for the flow rate were $7 * 10^{-7}$ mbar, $1.6 * 10^{-6}$ mbar and $5.0 * 10^{-6}$ mbar, a higher pressure indicating a higher flow rate. These pressures are referred to as the "low", "medium" and "high" flow settings.

Correcting these values for the initial background pressure we are left with $6*10^{-7}$ mbar, $1.5*10^{-6}$ mbar and $4.9*10^{-6}$ mbar. Due to the gas in question being hydrogen and due to the low pressures involved it is reasonable to treat it as an ideal gas. Using this assumption we can calculate the collision flux $Z = P / (2\pi\ m\ K_b\ T)^{1/2}$. As the mass m and temperature T are kept constant, Z is linearly dependent on the pressure P. For $P = 6*10^{-7}$ mbar we get

$Z = 6*10^{-7}$ [kg*m^{-1}*s^{-2}] / (2π*(1*10^{-3} [kg*mol^{-1}]/(6.6022*10^{-23} [mol^{-1}])) * 1.381*10^{-23} [J/K] * 293 [K])$^{1/2}$ = $9.669*10^{-7}$ [m^{-2}s^{-1}]

For $P = 1.5*10^{-6}$ mbar we get $Z = 2.417*10^{-6}$ [m^{-2}s^{-1}] and for $P = 5*10^{-6}$ mbar we get $Z = 7.896*10^{-6}$ [m^{-2}s^{-1}]. It is critical to note here that the atomic hydrogen is funnelled directly into the ion trap, while the pressures are measured at the walls of the chamber, and as such the pressure in the trap is significantly higher. Nonetheless, these flux values provide us with a relative chance of a hydrogen atom colliding with a PAH cation compared to other pressures.

For each of these pressures hydrogenation times of τ_{exp}=0, 0.1, 1, 5, 10, 20, 40 and 80 s were employed to investigate the effect of a variation in hydrogen fluence on superhydrogenation of coronene cations. If, for instance, the same ratios of hydrogenation states could be achieved by longer hydrogenation times at lower pressure, would there be other differences, such as a change in fragmentation?

Between τ_{exp}=5, 10, 20, 40 and 80 s the ratio between subsequent exposure times is always a factor 2. Multiplying these exposure times with the collision flux results in units of [m^{-2}], giving us an indication of the total number of collisions. Table 1 contains these multiplications of the Z and τ_{exp}.

Table 1	τ_{exp}=5 s	τ_{exp}=10 s	τ_{exp}=20 s	τ_{exp}=40 s	τ_{exp}=80 s
$Z = 9.669*10^{-7}$	$4.835*10^{-6}$	$9.669*10^{-6}$	$1.934*10^{-5}$	$3.868*10^{-5}$	$7.735*10^{-5}$
$Z = 2.417*10^{-6}$	$1.209*10^{-5}$	$2.417*10^{-5}$	$4.834*10^{-5}$	$9.668*10^{-5}$	$1.934*10^{-4}$
$Z = 7.896*10^{-6}$	$3.948*10^{-5}$	$7.896*10^{-5}$	$1.579*10^{-4}$	$3.158*10^{-4}$	$6.317*10^{-4}$

As table 1 indicates, combinations between high τ_{exp} and low Z, medium τ_{exp} and medium Z, and low τ_{exp} and high Z yield similar values, and should therefore be comparable. These sets of comparable values have been marked in the table. It should be noted that the high Z value yields a higher total number of collisions, and should therefore consistently yield a slightly higher hydrogenation rate than the medium and low Z values.

Figure 10 contains the hydrogenation states of coronene from τ_{exp}=5 s time at the highest pressure, τ_{exp}=10 s at the medium pressure and τ_{exp}=20 s at the lowest pressure, which have been normalised to the height of the middle mass peak, at 303 amu. Figure 11 contains the low mass fragmentation peaks, and figure 12 contains the C_2H_2 loss peaks.

Despite the total exposure value differing approximately a factor of 2 between the high pressure and low pressure measurement, the resulting hydrogenation states are highly comparable. Given the higher exposure value for the high pressure measurement, a higher degree of hydrogenation would be expected in a linear relationship, but is not observed here. It would appear that the hydrogenation states are not linearly dependent on the total number of collisions.

In figures 11 and 12 the black line, corresponding to the high pressure measurement, does show a higher degree of fragmentation at many peaks compared to the measurements at medium and low pressure, notably the 58, 60 and 74 amu and all C_2H_2 loss peaks. The higher fragmentation rate could be explained by more hydrogen atoms colliding with the coronene, depositing more energy in a shorter amount of time, which would lead to a higher occurrence of fragmentation.

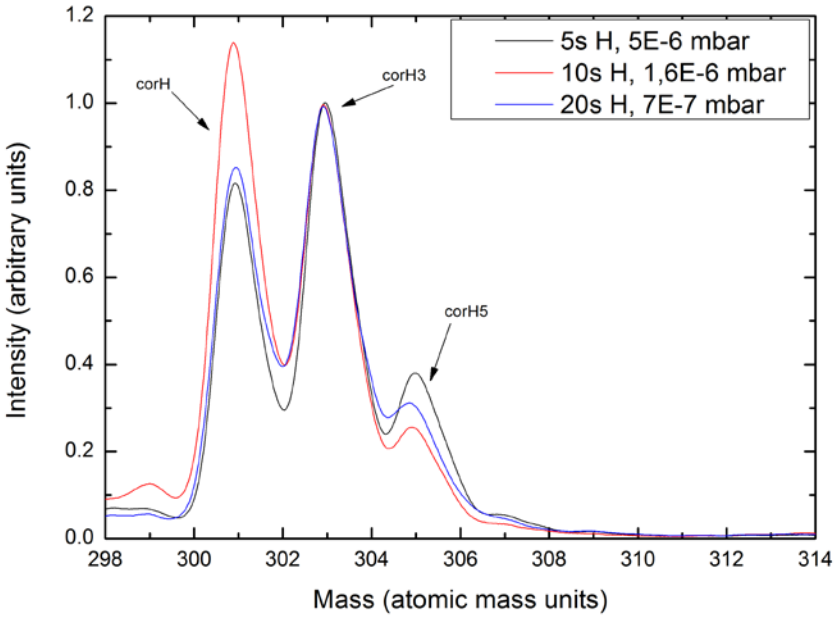

Figure 10: Graph comparing τ_{exp}=5 s at 5*10^{-6} mbar, τ_{exp}=10 s at 1.6*10^{-6} mbar and τ_{exp}=20 s at 7*10^{-7} mbar, which have been normalised to the height of the middle mass peak, at 303 mass.

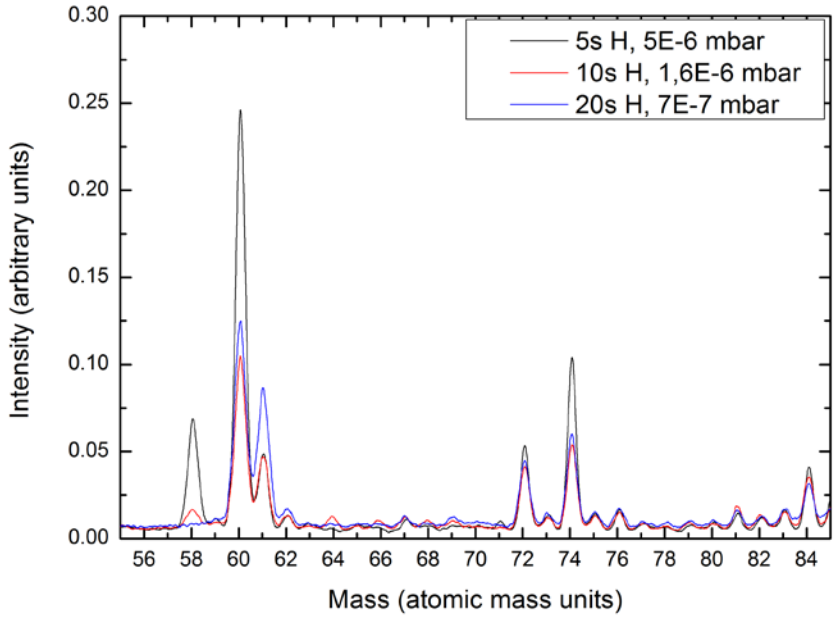

Figure 11: The low mass fragmentation peaks belonging to figure 10.

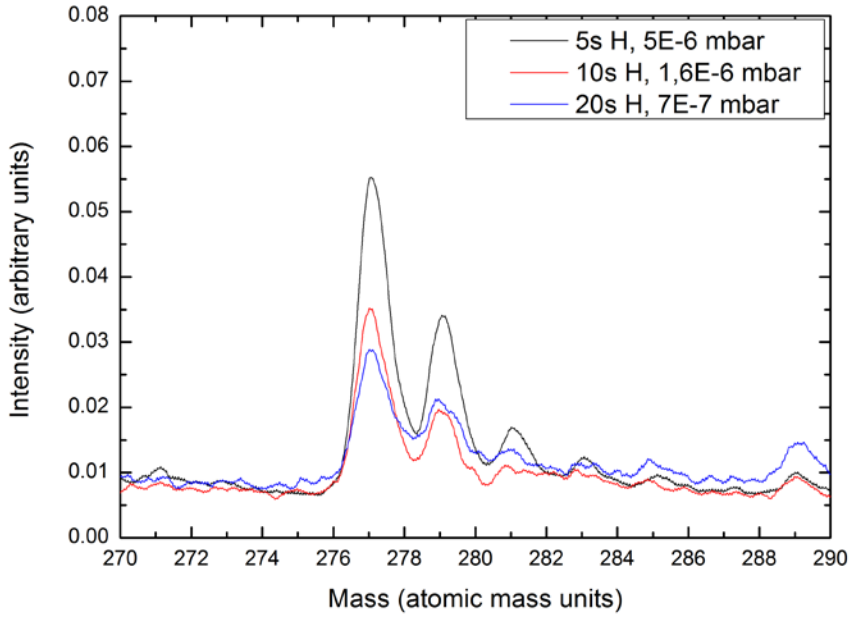

Figure 12: The high mass fragmentation peaks resulting from C_2H_2 loss, which belong to figure 10.

Figure 13 contains the measurement from τ_{exp}=10 s at the highest pressure, τ_{exp}=20 s at the medium pressure and τ_{exp}=40 s at the lowest pressure, which have again been normalised to the height of the middle mass peak, at 303 amu. At these exposure times the anticipated higher hydrogenation rate for the high pressure measurement appear to be more strongly manifested, with the hydrogenation peaks shifting more towards 305 amu and 307 amu.

Figure 14 contains the low end of the fragmentation spectrum resulting from these measurements, and figure 15 contains the C_2H_2 loss peaks. Examination of fig. 14 still shows a slight increase in low mass fragmentation for the high pressure measurement, but not as distinct as in figures 10 - 12. Fig. 15 shows a similar degree of C_2H_2 loss at high pressure compared to the lower exposure time measurements from fig. 12.

The overall rate of fragmentation has increased compared to the lower exposure time measurements, as is evidenced by the heights of fragmentation peaks in fig. 14 compared to hydrogenation peaks of fig. 13, compared to those of figs. 11 and 10. This is to be expected, as longer exposure times overall mean more impingements, and more energy being put into the coronene molecules.

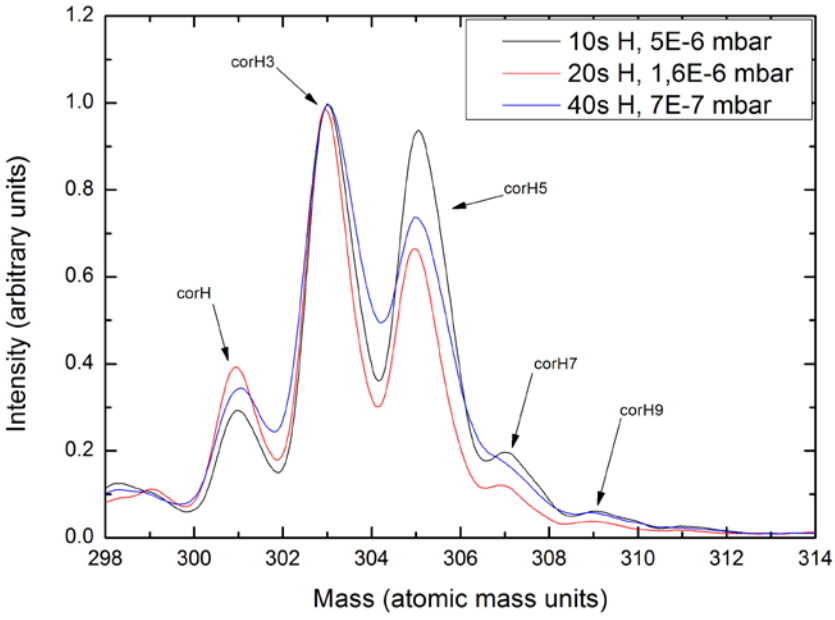

Figure 13: Graph comparing τ_{exp}=10 s at 5*10^{-6} mbar, τ_{exp}=20 s at 1.6*10^{-6} mbar and τ_{exp}=40 s at 7*10^{-7} mbar, which have been normalised to the height of the middle mass peak, at 303 mass.

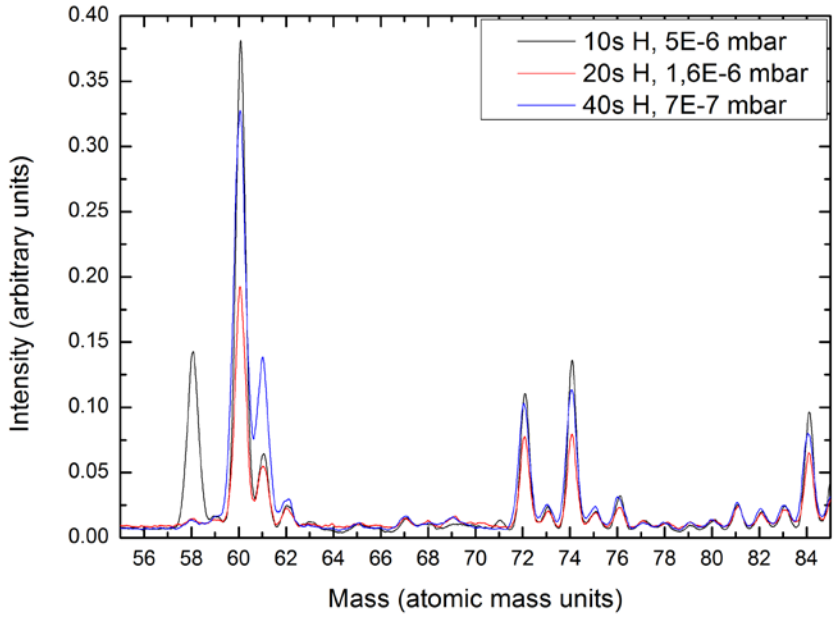

Figure 14: The low mass fragmentation peaks belonging to figure 13.

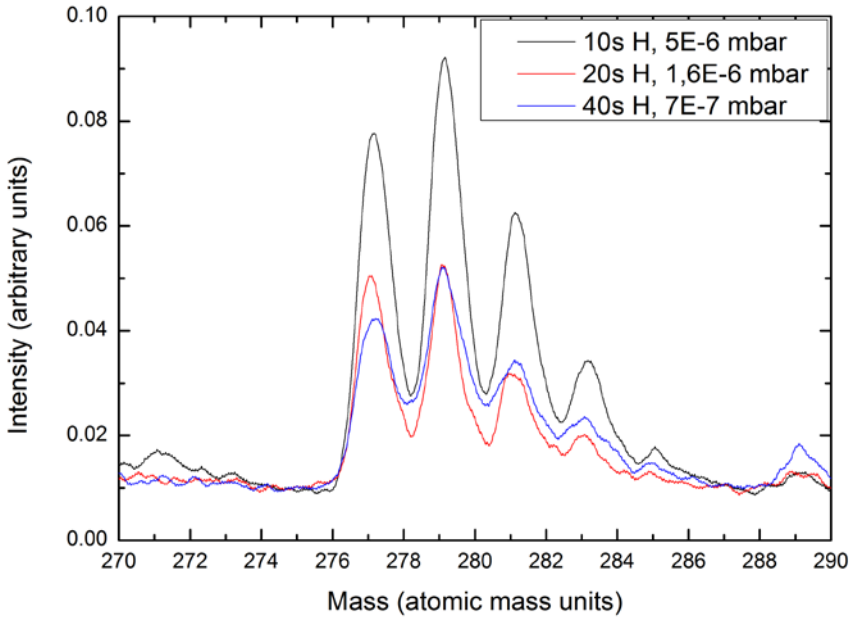

Figure 15: The high mass fragmentation peaks resulting from C_2H_2 loss, which belong to figure 13.

Figure 16 contains the measurement from τ_{exp}=20 s at the highest pressure, τ_{exp}=40 s at the medium pressure and τ_{exp}=80 s at the lowest pressure, normalised to the height of the middle mass peak, in this case 305 mass. At these higher exposure times the anticipated higher hydrogenation rate for the high pressure measurement does not appear to manifest itself at all. It appears, therefore, that the relation between the rate of exposure and resulting hydrogenation states is non-linear, becoming less efficient at higher fluence.

Figure 17 contains the low end of the fragmentation spectrum resulting from these measurements, and fig. 18 contains the C_2H_2 loss peaks. Here, however, the high pressure measurement does not appear to have undergone a significantly higher degree of fragmentation compared to the other two measurement. Even the C_2H_2 loss peaks do not exhibit any real differences between measurements.

It should be noted that the rate of fragmentation is again higher for all three measurements, the 60 amu fragmentation peak reaching an intensity of 0.6 to an intensity of 1 for the 305 amu hydrogenation peak. It appears, therefore, that the molecules receive more energy from the incoming hydrogen atoms in all cases and undergoing a higher degree of fragmentation, eliminating the effect of additional fragmentation for higher pressure measurements.

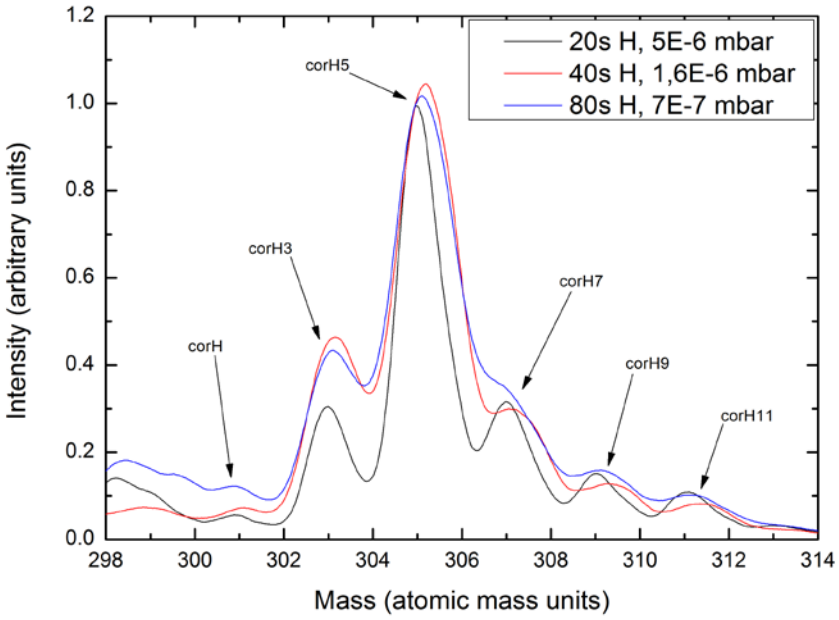

Figure 16: Graph comparing τ_{exp}=20 s at 5*10^{-6} mbar, τ_{exp}=40 s at 1.6*10^{-6} mbar and τ_{exp}=80 s at 7*10^{-7} mbar, which have been normalised to the height of the middle mass peak, at 305 mass.

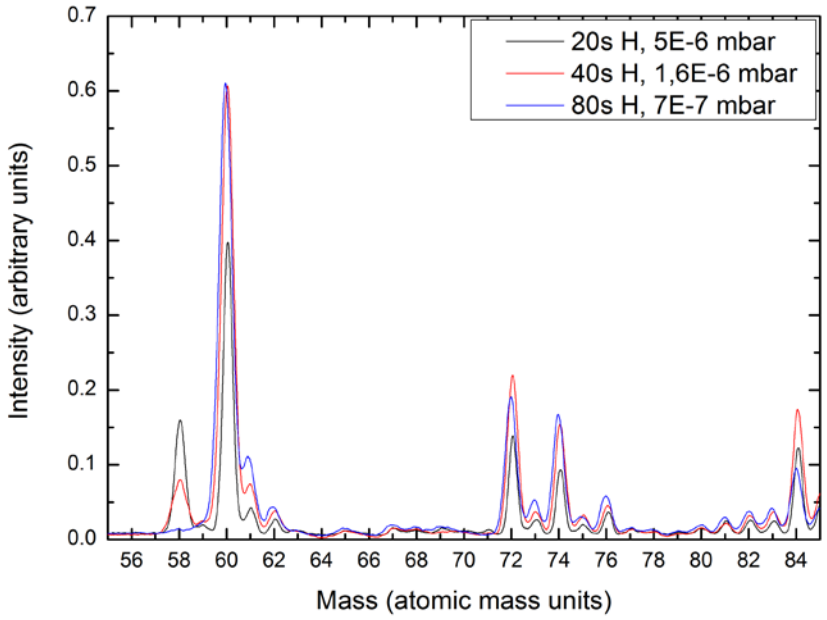

Figure 17: The low mass fragmentation peaks belonging to figure 16.

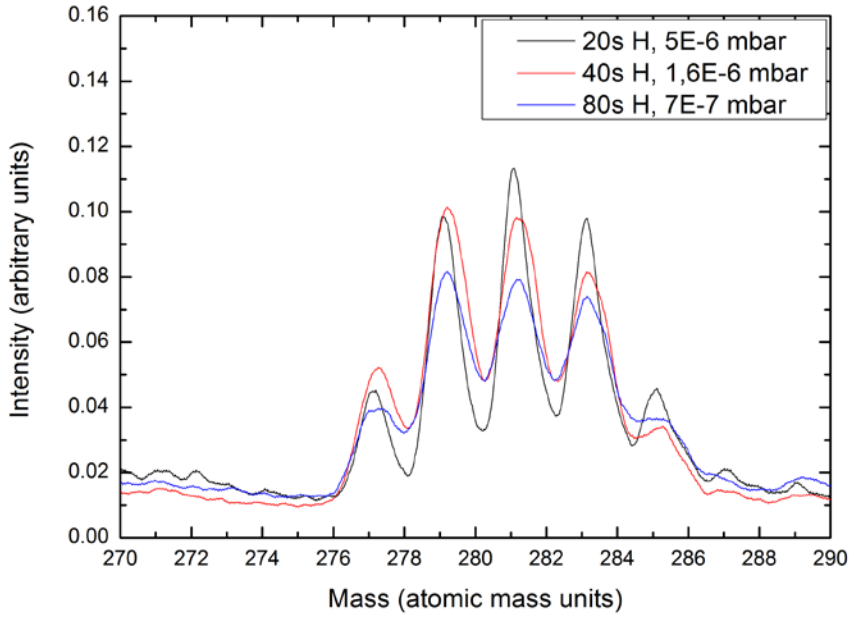

Figure 18: The high mass fragmentation peaks resulting from C_2H_2 loss, which belong to figure 16.

Experiments – deuteration of coronene

In previous studies on hydrogen attachment to coronene cations, adsorbed H atoms could not be distinguished from H atoms already present in the molecule, due to the lack of a measureable difference in mass. The following experiments therefore involved attaching deuterium (D) on coronene, instead of hydrogen (H). This was done in order to determine the prevalence of abstraction of H atoms attached to the coronene by incoming hydrogen or deuterium.

The hydrogenation of coronene follows the general reaction $C_{24}H_{(12+n)} + H \rightarrow C_{24}H_{(12+n+1)}$, where n is the hydrogenation state. Figures 19 and 20 show a sketch of a coronene molecule after respectively its first and second hydrogenation reaction. Hydrogenation of coronene cations leads to the appearance of odd-even oscillations in the resulting mass peaks, due to the energy barriers that arise at each addition of H. Every odd-numbered addition of hydrogen on the coronene cation has zero energy barrier, and every even-numbered addition has a small, but significant energy barrier, typically in the order of 30 – 100 meV [11]. This oscillating set of barriers originate from the electronic state of the PAH, as molecules prefer an even-electron-number state to an uneven (radical) state, where one electron is unpaired.

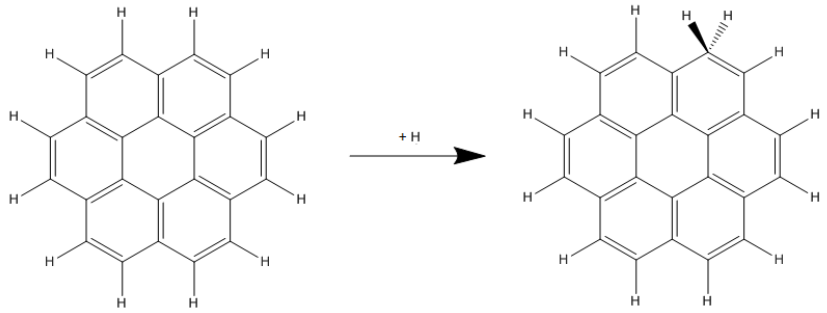

Figure 19: A sketch of the coronene molecule before and after a hydrogen atom addition reaction.

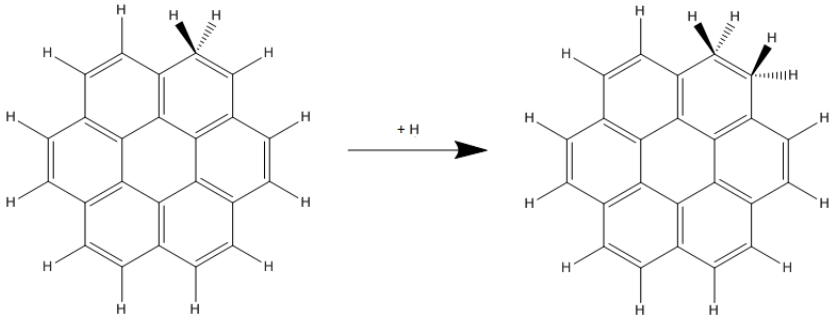

Figure 20: A sketch of the coronene molecule before and after a second hydrogen atom addition reaction.

Depending on the flux of atomic hydrogen this set of barriers results in strong peaks at 300 mass units for bare coronene, 301 for singly hydrogenated coronene, 303 for thrice hydrogenated coronene, and all subsequent odd numbers up until the coronene is fully saturated with 24 added hydrogen atoms and has a mass of 324 mass units. In fig. 21 we see the mass spectrum for bare coronene that has not undergone hydrogenation. We see a strong peak at 300 mass and a relatively small isotope peak at 301 mass, which was reduced as much as possible in order to obtain clear data

even for low intensity peaks. This level of accuracy had not previously been reached. There are also small contamination peaks present a 297, 298 and 299 mass, which remained a constant throughout the measurements.

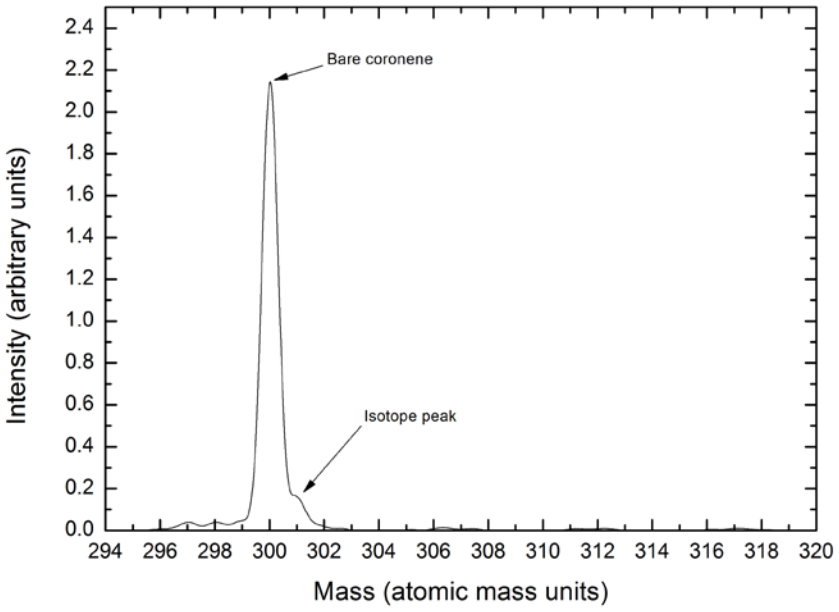

Figure 21: The mass spectrum of the reference measurement. The spectrum consists of the coronene mass peak at 300 amu with a relatively small isotope peak at 301 amu.

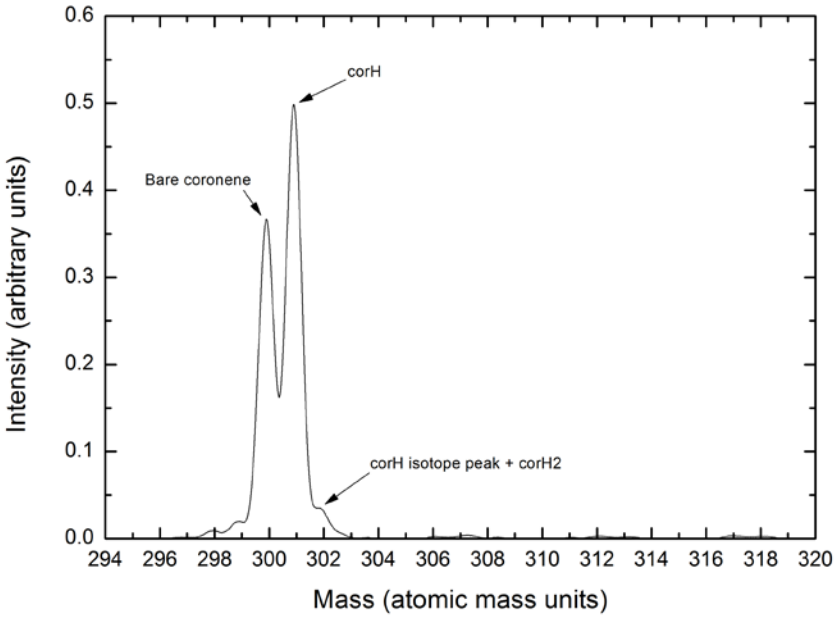

Figure 22: The mass spectrum of coronene after an exposure of τ_{exp}=0.15 s to atomic hydrogen at 1.5*10^{-6} mbar hydrogen background pressure.

The 300 and 301 peak for first hydrogenation can be seen clearly in figure 22, where coronene was exposed to atomic hydrogen for 0.15 seconds. Worth noting (but not shown) is that in these odd-numbered peaks there is another layer of magic numbering: the mass peaks for 5, 11 and 17 additions appear stronger than the other odd numbered peaks. This is due to relatively higher addition barriers for the 6th, 12th and 18th additions, compared to the other even numbered additions [11].

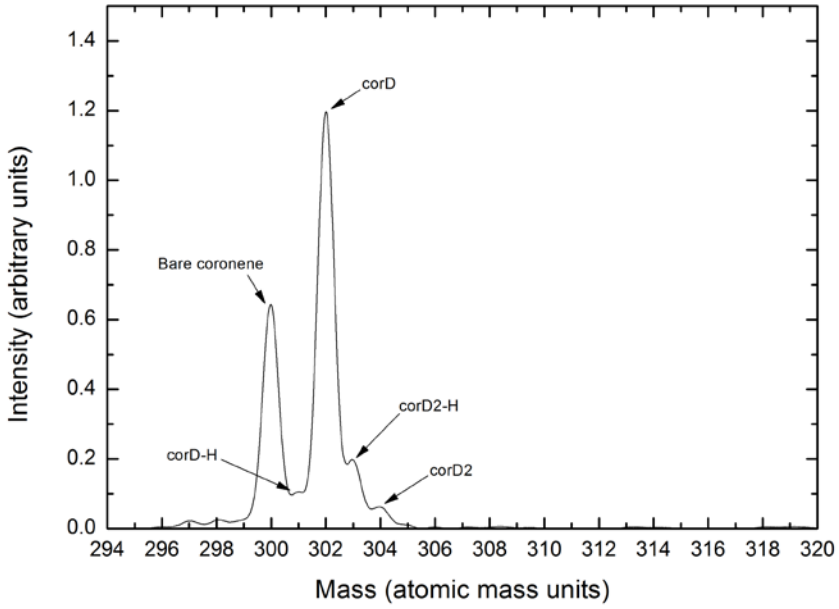

Figure 23: The mass spectrum of coronene after an exposure of τ_{exp}=0.15 s to atomic deuterium at 1.5*10^{-6} mbar deuterium background pressure.

The deuteration of coronene cations displays similar behaviour, and operates through the same mechanism. The peaks corresponding to odd numbers of addition have a high intensity, which is also down to the same barrier/no barrier system for even and odd numbered additions. Due to deuterium having a mass of 2 atomic mass units these addition peaks are seen at 302, 306, 310 and then every 4 mass units, again until saturation of the coronene molecule at a mass of 348. The 300 and 302 peak for first deuteration can be seen clearly in figure 23, which was measured under the same conditions as figure 22.

The labelling convention for deuterated coronene is identical the one used for hydrogenation, except the X in "corX" is replaced by the number of additional deuterium atoms attached to the molecule.

The sequence of hydrogenation differs significantly between neutral coronene, which to the author's knowledge has only been studied experimentally in thin films [6], and coronene cations, which are studied in gas phase [11]. Both neutral and ionic coronene have been studied through density functional theory (DFT) calculations. DFT calculations on neutral coronene indicate hydrogenation starts on an outer edge position, indicated in figure 24, where the first 2 H atoms will attach adjacent to each other and will deform that edge of the coronene from its planar configuration figure 25. From there on, the subsequent hydrogenation will occur on the neighbouring edge positions, and then on to the adjacent centre and further outer edge positions. The attachment process leaves the

outer edge C atom doubly occupied with H atoms, so a deformation from planar configuration results in a lower energy state for the molecule. The centre and edge positions can undergo attachment from either the “top” or “bottom” of the molecule [4,10].

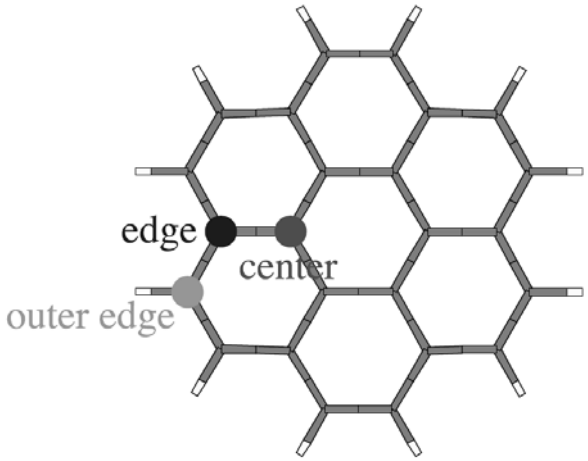

Figure 24: Possible attachment positions on a coronene molecule (source: adapted from ref. 10).

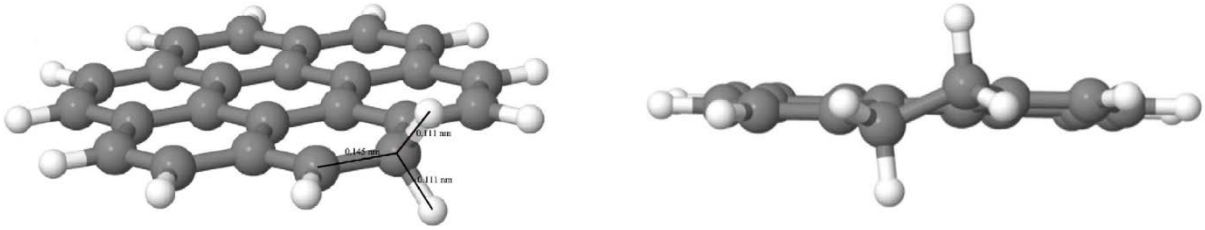

Figure 25: Deformation of a coronene molecule after addition of 1 (left) and 2 (right) hydrogen atoms (source: ref. 11).

DFT studies on coronene cations, however, indicate that the hydrogenation process works differently. The attachment process energetically favours the outer edge positions over the edge and centre positions. As such, after the first and second attachment, the third attachment will take place at one of the outer edge positions on an adjacent aromatic ring. The PAH cations also deform from their original planar configuration. A fully hydrogenated coronene cation has been determined to resemble alkane structures when viewed side-on [11].

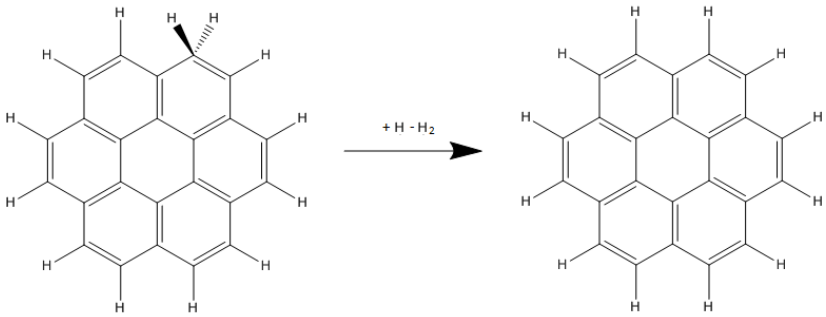

Figure 26: A sketch of the coronene molecule before and after a hydrogen atom abstraction reaction.

Besides addition, the abstraction reaction $C_{24}H_{(12+n)} + H \rightarrow C_{24}H_{(12+n-1)} + H_2$ can also occur. A sketch of hydrogenated coronene before and after the abstraction reaction can be seen in figure 26. In this reaction the incoming hydrogen atom impinges on the coronene and bonds with one of the

hydrogen atoms on a doubly occupied position of the molecule. This pair then detaches from the coronene as a H_2 molecule, leaving the system with one fewer hydrogen or deuterium atom. When hydrogenating coronene, the occurrence of abstraction reactions is impossible to gauge directly, as the addition of an H atom followed by its subsequent abstraction can not be told apart by mass spectrometry. It will simply appear as if neither reaction occurred, which could interfere with the investigation of the time evolution of the hydrogenation process if this potentially important process is not taken into account sufficiently.

Deuteration of the PAH is the only direct method for looking at abstraction reactions. Deuterium is electronically equivalent to hydrogen, which allows for a good comparison between hydrogenation and deuteration reactions. As the added deuterium atoms sit in aforementioned doubly occupied positions together with the originally present hydrogen atoms, an abstraction reactions has an approximately 50% chance to take either the deuterium or the hydrogen atom away. A deuterium-deuterium (D-D) abstraction, which follows the reaction $C_{24}H_{(12)}D_{(n)} + D \rightarrow C_{24}H_{(12)}D_{(n-1)} + D_2$, is similar to a hydrogen-hydrogen (H-H) abstraction, discussed earlier, in that it will appear as if the deuterium had never been attached to the coronene molecule in the first place. However, a hydrogen-deuterium (H-D) abstraction, following the reaction $C_{24}H_{(12)}D_{(n)} + D \rightarrow C_{24}H_{(11)}D_{(n)} + HD$, can be observed as it leads to a loss in mass of 1 amu, in an environment where the other reactions all lead to losses and gains of 2 amu. A sketch of a D-D abstraction reaction can be seen in figure 27 and a sketch of an H-D abstraction reaction can be seen in figure 28.

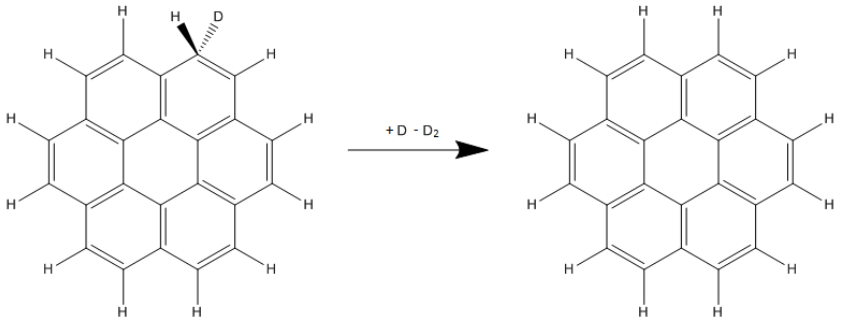

Figure 27: A sketch of the coronene molecule before and after a deuterium-deuterium abstraction reaction.

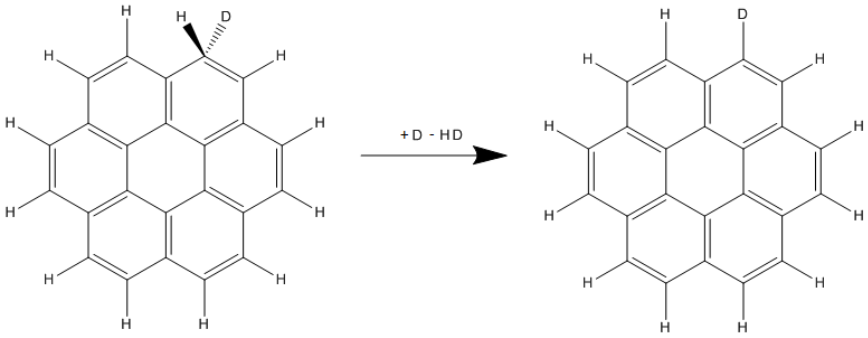

Figure 28: A sketch of an alternative outcome to the abstraction reaction depicted in fig. 27. Note that in this case the hydrogen atom was abstracted, and the deuterium atom remains on that location.

A consequence of H-D abstractions is not only that the molecule gains 1 amu compared to a molecule that did not undergo deuteration and subsequent abstraction, but also that that position of the molecule is now occupied by a deuterium atom, which may have consequences for probabilities

of any subsequent addition or abstraction reactions from that position. This is illustrated in fig. 29, as addition on this position results in it being doubly occupied by deuterium atoms. As a result, any abstraction from this position has to be D-D abstraction.

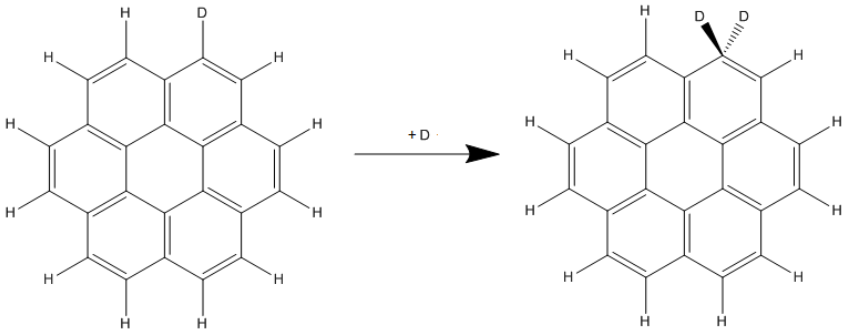

Figure 29: A sketch of a possible outcome to an addition reaction after the abstraction depicted in fig. 28. Note that it is not known whether the incoming deuterium atom will attach to this same position in this case, but it is one possible outcome.

The data obtained from the deuteration measurements clearly shows mass peaks that could only be formed through singular and even multiple abstraction reactions. To illustrate this, we shall analyse figures 30 and 31, which were obtained by respectively hydrogenating and deuterating coronene for τ_{exp}=3 s at 1.5*10^{-6} mbar. In figure 30 we see the mass peaks resulting from the hydrogenation. We see the main peak at 301 for singly hydrogenated coronene, a small peak at 302 for double hydrogenation, and a slightly larger peak at 303 for triple hydrogenation. In figure 31 we see the mass peaks resulting from the deuteration under the same conditions. We also see the main peak for single deuteration, here at 302 mass, we see a double deuteration peak at 304 mass, and a larger peak at 306 mass for triple deuteration. However, the 304 peak is stronger than one would expect for just double deuteration, and there are strong peaks present at 303, 305, 307 and 308, and minor peaks at 301, 309 and 310, which have no analogue in the hydrogenation measurement. Furthermore, the ratio between the two main peaks is not equal between the two figures, despite the circumstances of the measurements having been identical.

The height of the 304 mass peak in fig. 31, relative to the hydrogenated 302 peak in fig. 30, indicates that it can not be caused solely by double deuteration. The presence of mass peaks at 303, 305, 307 and 309 in fig. 31 show that the addition reaction by itself can not describe the hydrogenation or deuteration process. These masses can only be reached by a number of abstraction reactions following additions. For instance, the 303 peak is likely to arise from two additions and one H-D abstraction. It should also be noted that these peaks can only result from H-D abstractions, so assuming D-D and H-D abstractions are equally likely for a given deuterated position on the PAH molecule, abstraction should occur twice as often as these graphs would suggest. As discussed earlier, it is possible that H-D reactions could lead to a higher occurrence of D-D reactions after subsequent additions, and that as a result D-D abstractions are more prevalent still, but we can not currently make any hard estimates to this effect.

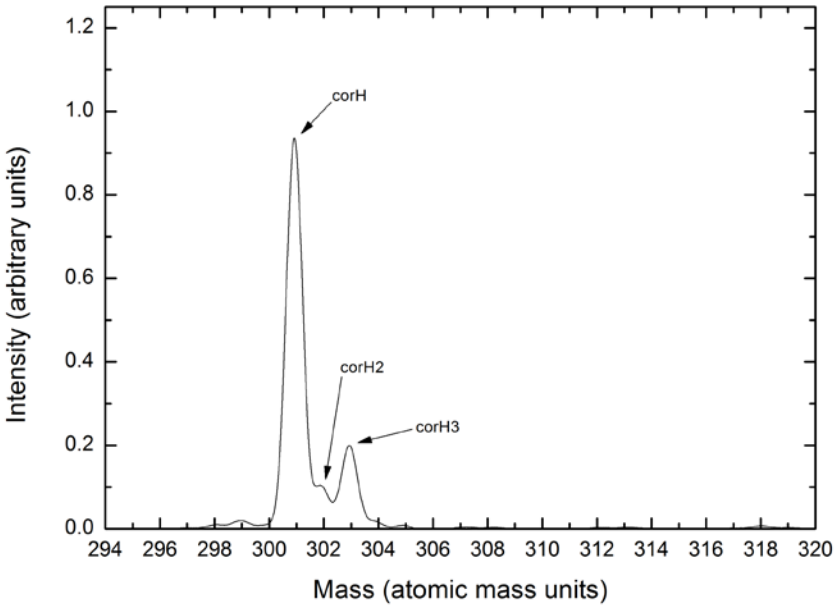

Figure 30: The mass spectrum of coronene after an exposure of τ_{exp}=3 s to atomic hydrogen.

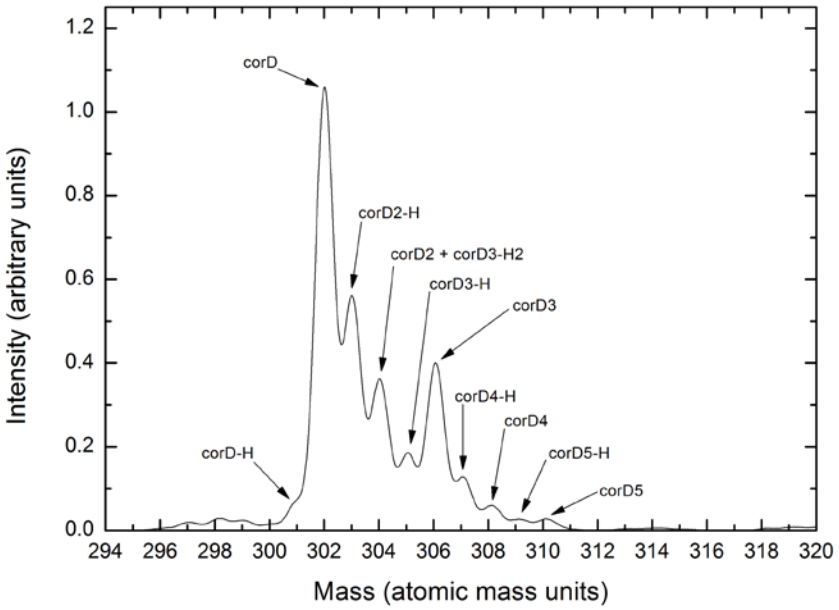

Figure 31: The mass spectrum of coronene after an exposure of τ_{exp}=3 s to atomic deuterium.

Figures 32 and 33 are the result of respectively hydrogenating and deuterating coronene for 9 seconds at $1.5*10^{-6}$ mbar. In figure 32 we can clearly see the three main peaks at 301, 303 and 305 amu, corresponding to 1, 3 and 5 attached hydrogen, and smaller peaks at 302, 304, 306 and 307 mass corresponding to 2, 4, 6 and 7 attached hydrogen atoms. In fig. 33 we see peaks at every mass between 302 and 315. Here the peaks corresponding to 1, 3 and 5 attached deuterium are located at

302, 306 and 310 amu. However, the differences between these two figures are immediately clear – the ratios between the main peaks do not correspond at all.

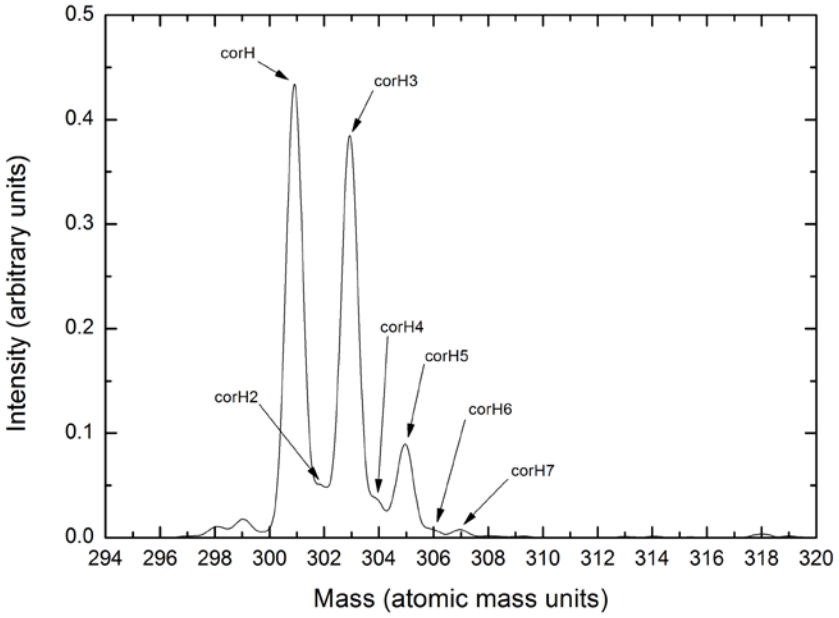

Figure 32: The mass spectrum of coronene after an exposure of τ_{exp}=9 s to atomic hydrogen.

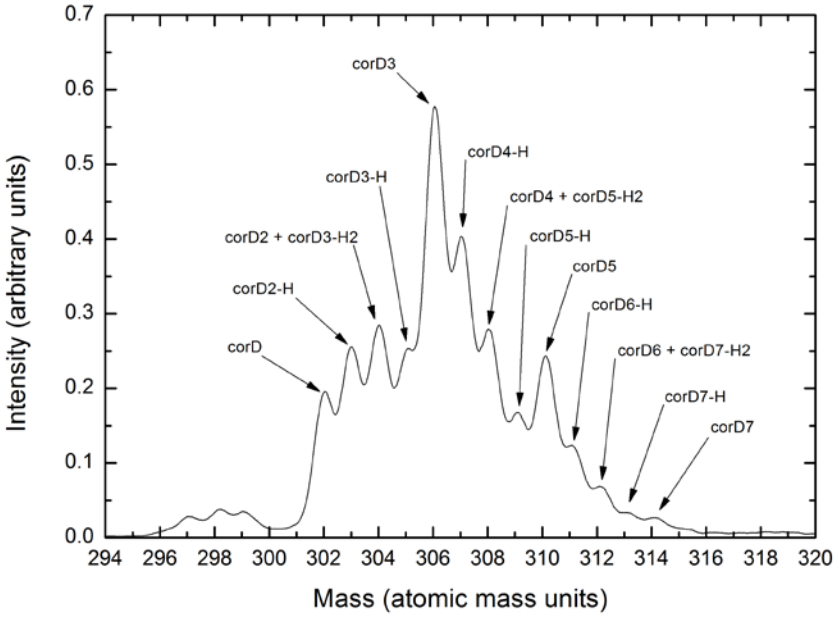

Figure 33: The mass spectrum of coronene after an exposure of τ_{exp}=9 s to atomic deuterium.

Fig. 34 illustrates the reaction pathways that can be taken during deuteration of coronene up to the 306 mass peak. The illustration starts at the upper left, with bare coronene at 300 amu. From there, either addition (+D) or abstraction (+D-D_2 / +D-HD) can take place, resulting in the various contributing states of deuteration of each mass peak. There are 63 reaction pathways depicted, which is the minimum number necessary to take into account all four states of deuteration that can contribute to the 306 mass peak. In order to identify the contributors to the next mass peak another diagonal row of reaction pathways must be added, each added row containing three more reactions than the last, until the fully hydrogenated state of coronene at 348 mass units is reached. This gives a total of 900 reaction pathways. It should be noted that this number does not take into account the different isomers of each deuteration state of the coronene, where additions and abstractions have taken place on different positions on the molecule. These isomers may affect the electronic state of the PAH, and therefore the probability of either abstraction or addition reactions taking place at certain positions.

One should keep in mind that it is the number of doubly occupied positions that determines the electronic structure of the molecule, and not whether these positions are occupied by H or D atoms. As such, coronene that has undergone four D addition reactions and three H-D abstractions, resulting in 305 amu, still only has one doubly occupied position, and is therefore in the same electronic state as coronene that has undergone 1 addition (302 amu). The same goes, for example, for 2 additions and 1 H-D abstraction (303 amu), and 5 additions and 4 H-D abstractions (306 amu), though the amount of reactions required by the latter make it less probable. This is how these “new” mass peaks appear under deuteration.

During hydrogenation there are obviously no deuterium atoms present for H-D abstractions to take place. As such, mass peaks resulting from H-D abstractions in deuteration experiments manifest as additional peak intensity on the mass peak corresponding to the same number of doubly occupied positions in hydrogenation experiments. So for instance the 302, 303 and 305 amu deuteration peaks, and a portion of the 304 amu peak that is not attributed to double deuteration, all correspond to 1 doubly occupied position on the coronene cation. In a hydrogenation experiment these peaks are merged into the 301 amu peak.

For neutral coronene the addition and abstraction reaction cross sections have been calculated based on deuteration and hydrogenation of coronene in a thin film [6]. These cross sections were 1.1Å^2 and 0.06Å^2 for addition and abstraction respectively, giving a ratio of about 20:1. However, coronene cations have already been shown to undergo the addition reaction of hydrogen in a completely different way than neutral coronene [11], so it is possible that abstraction reactions also occur with some fundamental differences. Furthermore, as coronene molecules have been shown to undergo significant deformation after hydrogenation, twisting out of its regular planar configuration, conducting such experiments on coronene which has been deposited on a surface, and may thus be inhibited in its ability to deform, may have an impact on the hydrogenation and abstraction processes. This surface could also slightly alter the electronic structure of the coronene, and given that the reaction barriers are only a few meV high, even a subtle change to the electronic structure could alter the hydrogenation properties noticeably. Furthermore, PAH molecules in a film interact with each other through the formation of bonds, and only one face of the molecule is exposed to the incoming hydrogen, so addition and abstraction reactions are likely to be strongly affected by this environment. Great care has to be taken, when comparing this to DFT results for “free” molecules.

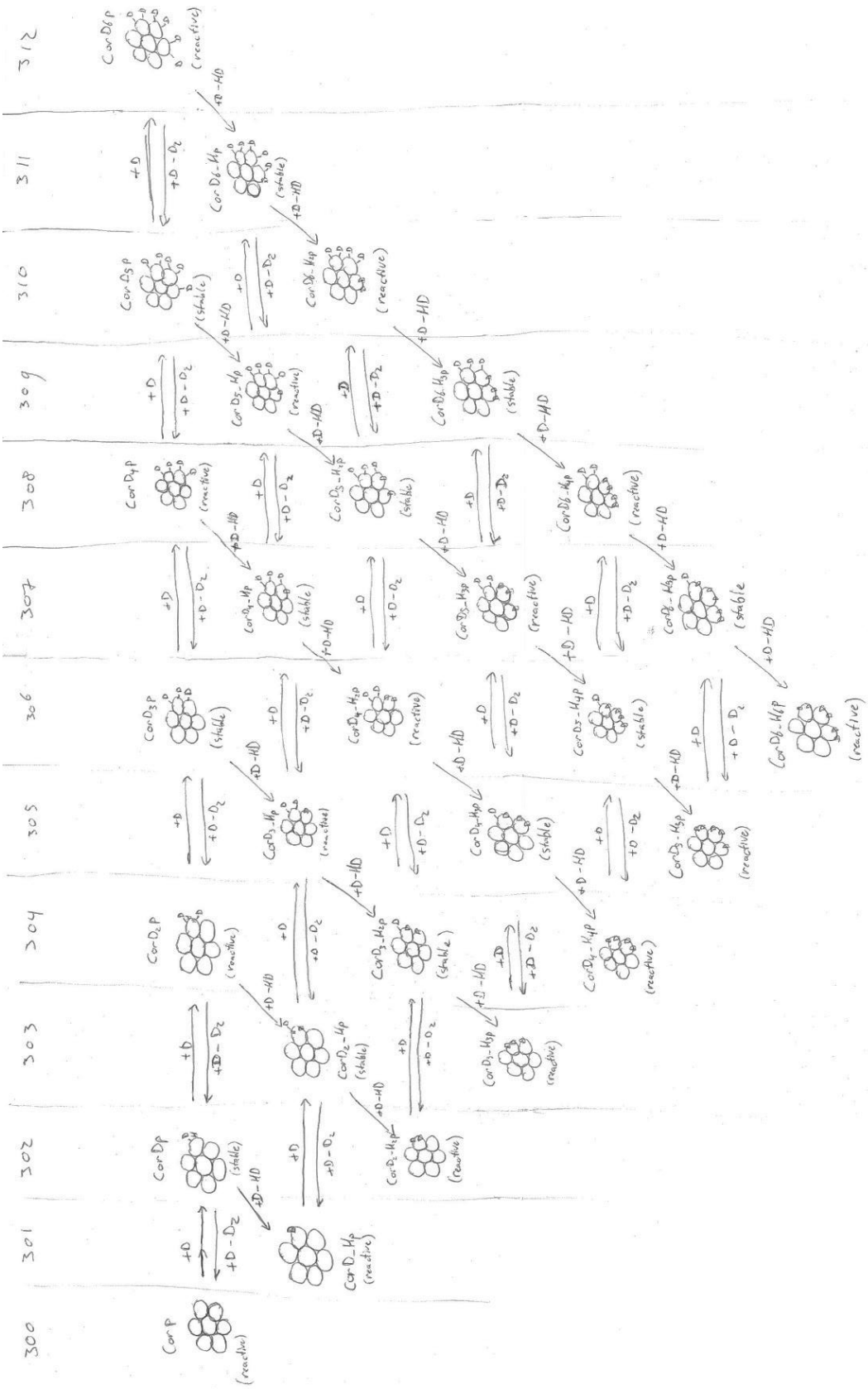

Figure 34: Illustration depicting the reaction pathways necessary for identifying the possible reaction pathways resulting in the 306 amu peak, for deuteration of a coronene sample. Also depicted is whether each deuteration state is relatively reactive or relatively stable, based on the electronic state of the molecule.

It should be noted that, despite ongoing DFT calculations, there is currently not enough information about what the positional preferences are for abstraction reactions or addition reactions following abstractions. For example, a doubly hydrogenated coronene cation can undergo abstraction from either of the doubly occupied positions and, given that these positions are under the same conditions with respect to the electronic structure of the molecule, these abstraction reactions are likely to have a 50/50 probability. On coronene that has undergone 3 addition reactions the probabilities become far less obvious. While we know that during addition the third incoming hydrogen atom will attach to an outer edge position on an adjacent aromatic ring, we do not currently know whether this third hydrogen atom has a higher likelihood of being abstracted. In the case that one of the first two added hydrogen atoms is abstracted, does this position then have a higher likelihood of undergoing addition than a given other position on the molecule? Do H-D abstractions, leaving the previously doubly-occupied position with one attached deuterium atom, influence subsequent additions and abstraction probabilities? If this position undergoes another addition it will be doubly occupied with deuterium atoms, resulting in the same mass as a molecule with more doubly occupied positions, but with fewer positions from which abstraction can occur.

While the system is highly complex, ultimately there are a finite number of possible configurations for hydrogen on a coronene molecule, and as such it can be solved with additional experiments and modelling. However, current analysis of the experimental data is severely limited by these uncertainties and lack of understanding of the ongoing processes.

Given these limitations, we aimed to get a bandwidth of realistic ratios between addition and abstraction cross sections. A model was made to calculate the reaction cross sections up to 306 mass units for deuteration. This was done based on possible reaction pathways, reaction barriers which have been calculated using DFT, and the mass peak intensities obtained during the measurements. The mass peaks from each measurement were fitted using Origin graphing software. Using the ratio between the minimised 301 peak and the 300 peak, the contribution of the isotope peak, though minimal, to each mass peak could be taken into account and corrected for. The resulting data was used in the model.

Literature values for addition and abstraction barriers for hydrogen atoms on coronene cations, calculated through DFT [12], can be found in table 2. These values will be same for deuterium addition and abstraction, but the notation method in the tables is for hydrogenated coronene, in order to avoid the more complex notations that would result from H-D abstractions in deuterated coronene. It should be noted that the abstraction barrier for Cor+ and the addition barrier for $CorH_6$+ have been omitted, as they are not relevant to the model. These barriers gave an average addition to abstraction reaction cross section ratio of 10.5:1.

Table 2	Addition Barrier (meV)	Abstraction Barrier (meV)
Cor+	0-10	
CorH+	28	0
$CorH_2$+	0	10
$CorH_3$+	46	0
$CorH_4$+	0	10
$CorH_5$+	64	0
$CorH_6$+		10

However, the model produces fits that are in poor agreement with experimental results when using these barrier values, as can be seen in figure 35. A likely explanation for this is that these barriers were calculated under the assumption that abstraction reactions on cations have the same relatively small cross section as on neutral coronene. As such, the model was run with a wide variety of different configurations of abstraction barriers, such as matching the abstraction and addition barriers, raising all abstraction barriers equally, or raising and lowering individual barriers. This was done until the best resulting fit was obtained, which can be seen in fig.36. The barriers used for this can be found in table 3. These barriers gave an average addition to abstraction reaction cross section ratio of 1.6:1.

Table 3	Addition Barrier (meV)	Abstraction Barrier (meV)
Cor+	10	
CorH+	30	50
$CorH_2$+	10	10
$CorH_3$+	46	80
$CorH_4$+	10	10
$CorH_5$+	64	100
$CorH_6$+		10

From here on, we decided to continue to run the model with higher barrier values for addition in order to see at what point the resulting fit is no longer in good agreement with the experimental data. The highest set of barriers that still resulted in a decent fit can be found in table 4. These barriers gave an average addition to abstraction reaction cross section ratio of 2.5:1. The resulting fits can be found in fig.37.

Table 4	Addition Barrier (meV)	Abstraction Barrier (meV)
Cor+	10	
CorH+	50	50
$CorH_2$+	10	10
$CorH_3$+	80	80
$CorH_4$+	10	10
$CorH_5$+	110	110
$CorH_6$+		10

Examining these different results of the model we find that, regardless of which set of barriers are used, the cross section for abstraction has been significantly underestimated in previous studies. Even for a 0 meV abstraction barrier the ratio between addition and abstraction cross section is almost double that previously reported, at 10.5:1 to 20:1. However, selecting abstraction barriers that reproduce experimental data more closely gives ratios close to or even exceeding 2:1, indicating a full order of magnitude higher probability of abstraction taking place. This could have substantial implications for H_2 formation in space.

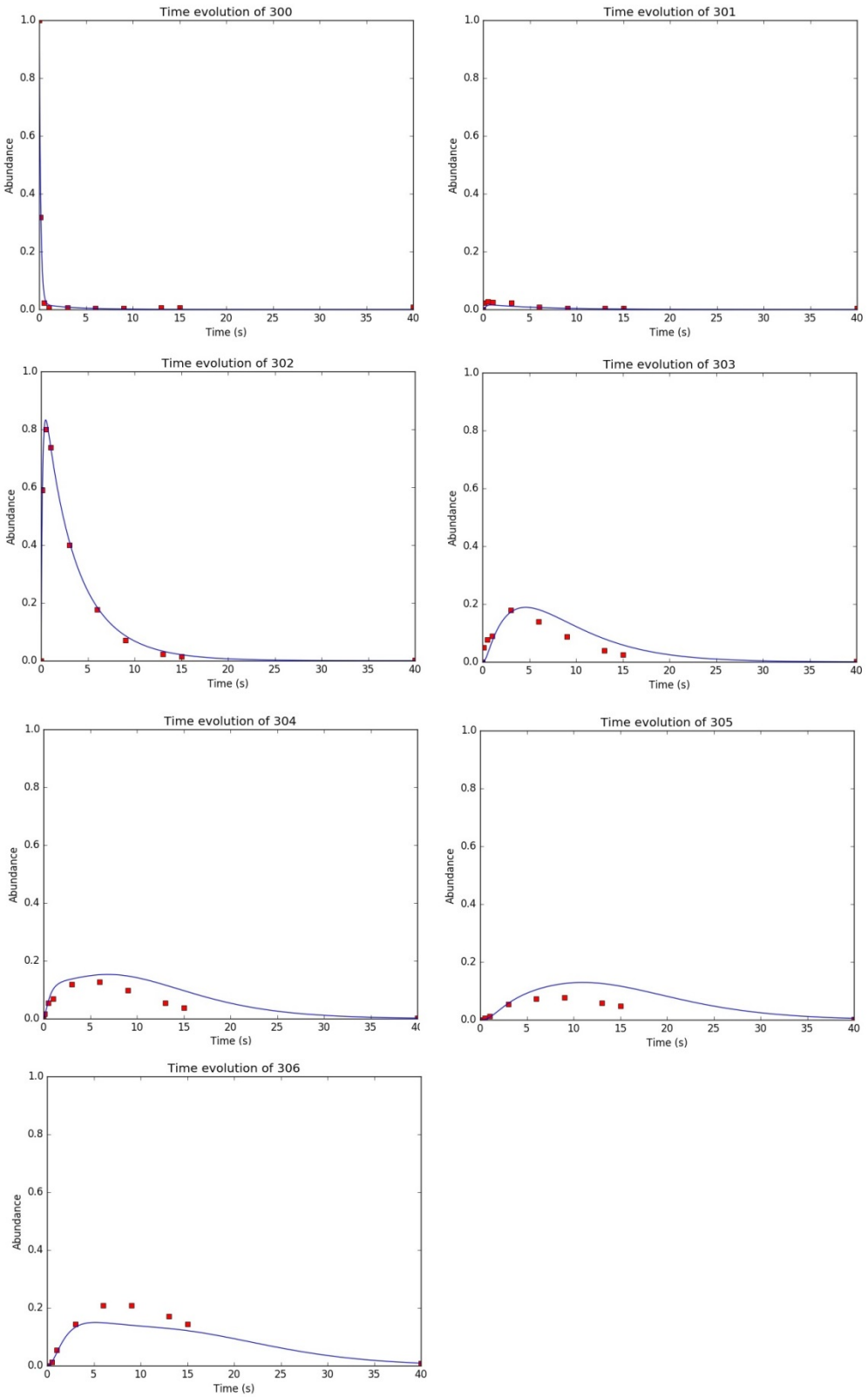

Figure 35: Fit resulting from running the model based on literature values for reaction barriers, found in table 2.

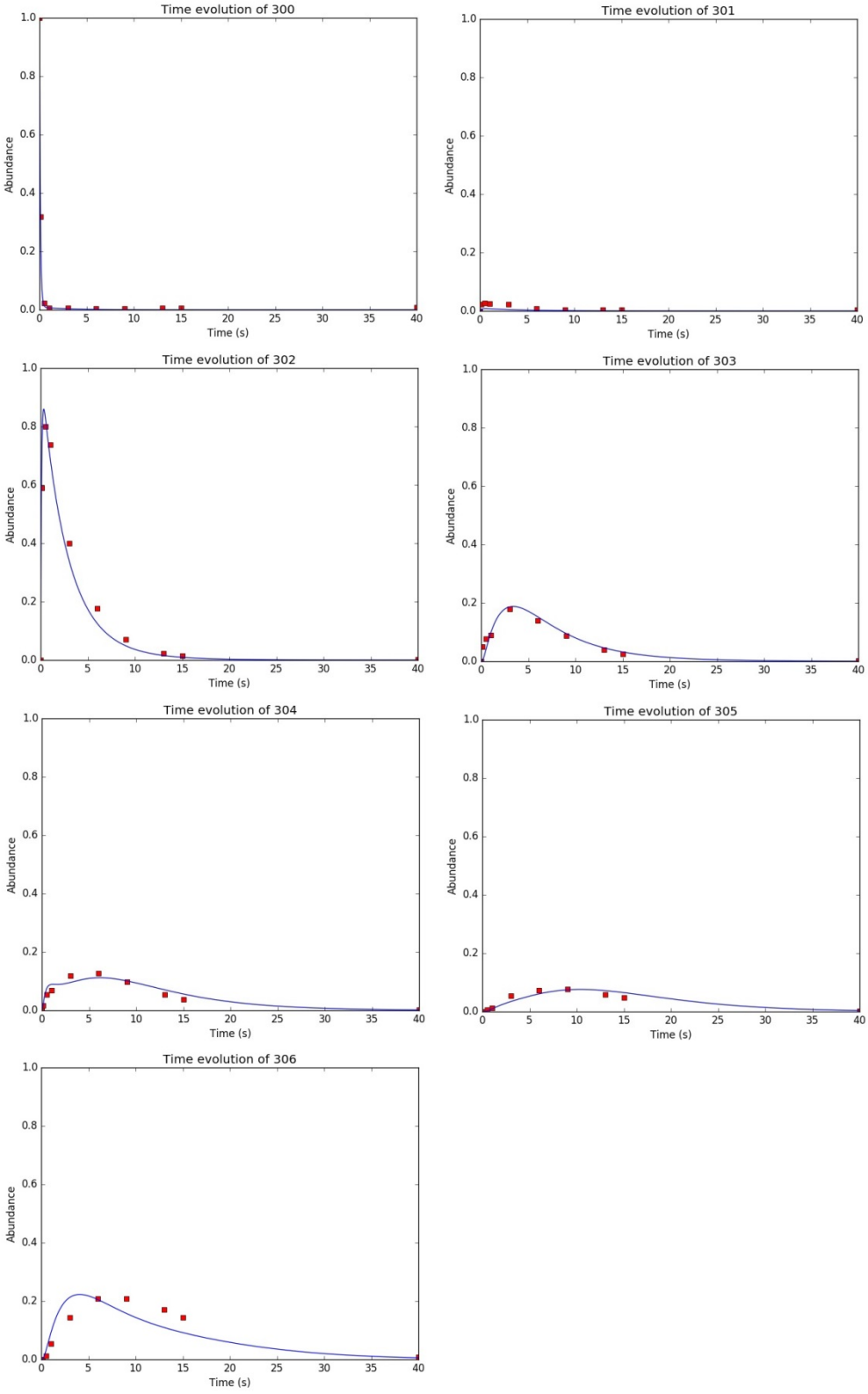

Figure 36: Fit resulting from running the model based on reaction barriers found in table 3.

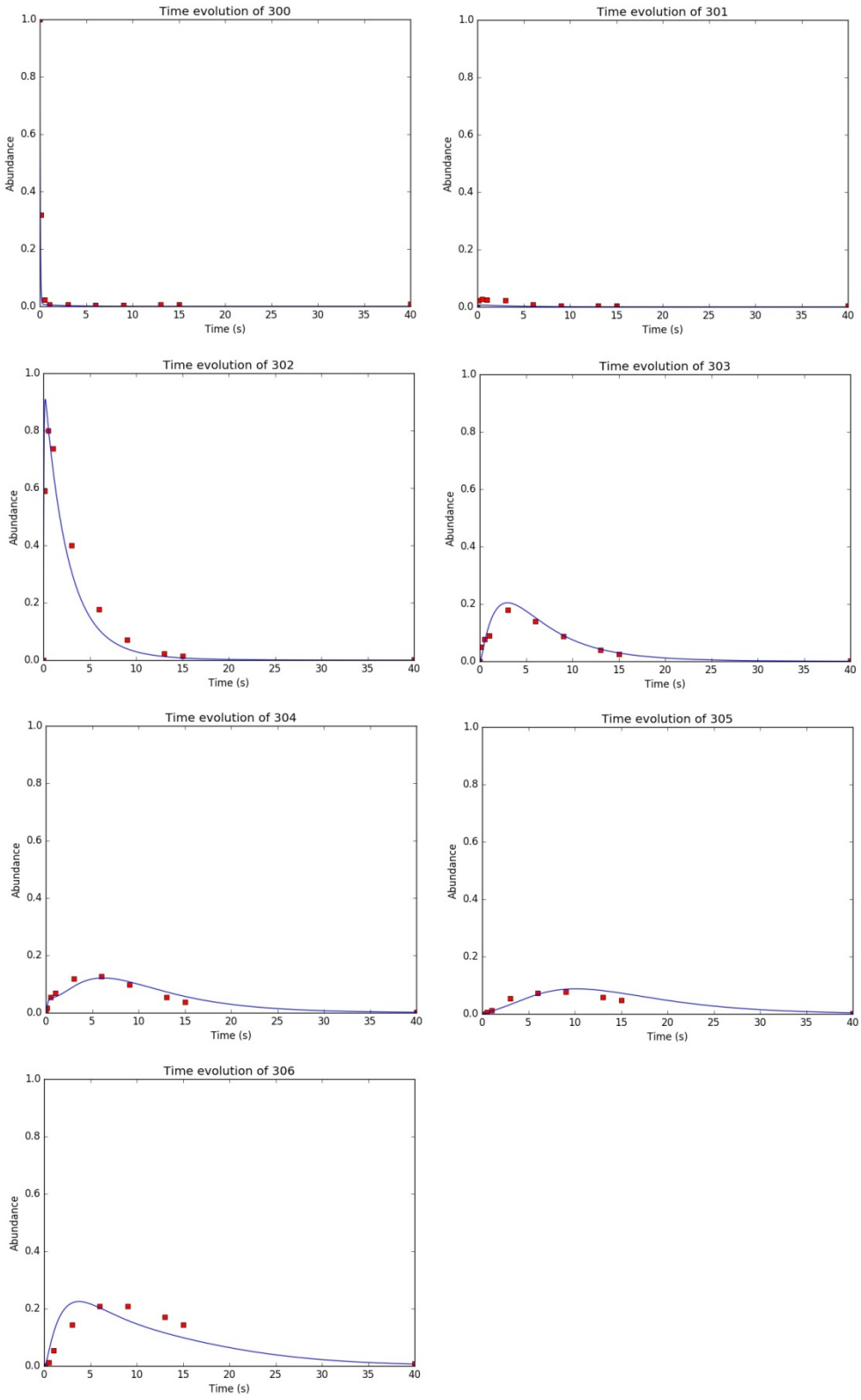

Figure 37: F it resulting from running the model based on reaction barriers found in table 4.

Conclusion

To summarise the different experiments conducted:

The measurements conducted to investigate the occurrence of a desorption mechanism on hydrogenated coronene found that a reduction in height for certain mass peaks occurred after holding the molecules in the ion trap after hydrogenation, but did not find an increase in bare coronene mass peak that would correspond to a desorption reaction. It did, however, find an increase in low mass fragmentation peaks, suggesting that the loss in signal is due to an increased ratio of fragmentation after holding the molecule. However, the process at work here is unclear and requires further investigation.

Investigating the effect of atomic hydrogen fluence, or the rate at which atomic hydrogen impacts on a PAH molecule, revealed that a higher fluence leads to a higher rate of fragmentation at lower hydrogenation times, but that for longer hydrogenation times the difference was mainly lost, possibly due to fragmentation occurring more frequently for all fluence settings. It also appeared that an increase in atomic hydrogen fluence does not result in a linear increase in hydrogenation of the coronene sample.

Studying the prevalence of abstraction reactions through deuteration of coronene yielded something of a surprise. Abstraction cross section seem to be about one order of magnitude higher than suggested by previous studies. While earlier measurements on neutral coronene in thin film gave the ratio between abstraction to addition cross sections to be around 1:20, suggesting a relatively low prevalence, our measurements on gas phase coronene cations immediately show the effects of a commonly occurring abstraction reaction. By fitting a model to the mass peaks resulting from abstraction and addition reactions, a bandwidth for estimates of the ratio between abstraction and addition cross sections could be formed, with the lower estimate being around 1:10 and the higher estimate exceeding 1:2. It should be noted that due to the current lack of knowledge on the effects of abstraction and addition reactions on each other and not being able to measure H-H or D-D abstractions directly, it is possible that abstraction reactions are even more common than indicated here.

Appendix – Improving the quality of the coronene samples

The PAH samples studied in Paultje are created by dissolving the PAH in methanol, and ionising it with an ionisation agent, dependent on the PAH. In the case of coronene the ionisation agent used is either zinc nitrate ($Zn(NO_3)_2$) or silver nitrate ($AgNO_3$).

However, a large issue with this method is that methanol is simply not a good solvent for PAHs. This results in a very low concentration of PAH in samples, and subsequently a low signal, or an unstable signal, as the PAH could cluster together, or inside the tube of the ion spraying device. An unstable signal is highly undesirable for measurements over long periods of time, and as such an improvement for the samples was sought.

A problem when working with PAHs is that they are generally poorly soluble in solvents used for electrospraying [16]. The current method for sample fabrication involves pipetting from a saturated solution of coronene in methanol, which is both fairly imprecise and can result in aforementioned issues, but in order to be able to fully dissolve a given measurable amount of coronene more potent solvents are required. In this case, dichloromethane (DCM) was selected, due to its ability to dissolve a wide selection of organic compounds, including plastics. Working with DCM does give rise to a number of complications.

A primary concern are the health risks associated with DCM. It is carcinogenic and toxic, and due to its high volatility is an acute inhalation hazard. As such, lab personnel working with DCM are required to wear half-face masks specifically made for dealing with organic gasses even while working under a fume hood. Furthermore, DCM can be absorbed through the skin, and neoprene do not sufficiently protect one from DCM, so the safety protocol advises immediate removal of the gloves and thorough washing of the skin if any DCM is spilled on them.

Other complications arise from the fact that DCM is such a good solvent. Both the pipette tips are sample cups are made out of polyethylene, and sources disagree on how soluble this is in DCM. The sample cups were replaced by glass vials with Teflon inserts in the caps, but the pipette tips were deemed usable due to the DCM not being in contact with them for long.

Initial tests for sample preparation with DCM were done with pyrene, a smaller PAH than coronene, consisting of 4 benzene rings. While pyrene is more easily soluble than the larger PAHs, it remains comparable to coronene in methanol. The solubility in DCM is evidently far higher, as the pyrene was fully dissolved upon deposition into the solvent. Prior to dissolution in DCM the pyrene was weighed, allowing the derivation of the sample's concentration.

Attempting the same sample preparation method for coronene and visually inspecting the result gave a clear, slightly yellow solution, with seemingly close to the entirety of the deposited coronene precipitating to the bottom of the vial. Neither shaking, nor waiting for a number of weeks appear to have changed the composition of the mixture, indicating that coronene is simply very poorly soluble, even in DCM.

Given the complications of working with DCM, this result was deemed too impractical for further investigation, and the author returned to the previous imperfect-but-functional method of sample preparation.

The original recipe utilised silver nitrate as ionisation agent, but this was substituted for zinc nitrate, which resulted in a marked increase in signal strength and stability. The samples prepared in this manner proved to be very reliable and were utilised for all experiments described in this thesis.

References

1. Oort, J. H. & Van de Hulst, H. C. 1946, Bull. Astron. Inst. Neth, 10, 187.
2. Gould, R. J., & Salpeter, E. E. 1963, ApJ, 138, 393
3. Bauschlicher, Jr., C. W. 1998, ApJ, 509, L125
4. Hirama, M., Tokosumi, T., Ishida, T., & Aihara, J. 2004, Chem. Phys., 305, 307
5. Le Page, V., Snow, T. P., & Bierbaum, V. M. 2009, ApJ, 704, 274
6. Mennella, V., Hornekær, L., Thrower, J., & Accolla, M. 2012, ApJ, 745, L2
7. Boschman, L., Reitsma, G., Cazaux, S., Schlathölter, T., Hoekstra, R., Spaans, M., & González-Magaña, O. 2012 ApJL 761, L33
8. Schutte,W. A., Tielens, A. G. G. M., & Allamandola, L. J. 1993, ApJ, 415, 397
9. Bernstein, M. P., Sandford, S. A., & Allamandola, L. J. 1996, ApJ, 472, L127
10. Rauls, E., & Hornekær, L. 2008, ApJ, 679, 531
11. Cazaux, S., Boschman, L., Rougeau, N., Reitsma, G., Hoekstra, R., Teillet-Billy, D., Morisset, S., Spaans, M. & Schathölter, T. 2016 Scientific Reports 6, 19835
12. Boschman, L., Cazaux, S., Spaans, M., Hoekstra, R. & Schlathölter, T. 2015, A&A 579, A72
13. Jochims, H. W., Ruhl, E., Baumgartel, H., Tobita, S., & Leach, S. 1994 Astrophys. J. 420, 307
14. Ling, Y. & Lifshitz, C. 1998 J. Phys. Chem. A 102, 708
15. Reitsma, G., Boschman, L., Deuzeman, M., González-Magaña, O., Hoekstra, S., Cazaux, S., Hoekstra, R. & Schlathölter, T. 2014, Physical Review Letters, 113, 053002
16. https://en.wikipedia.org/wiki/Coronene (last accessed June 2016)
17. Slevin, J. & Stirling, W. 1981, Rev. Sci. Instrum. 52 (11), 1780